CHALMERS
UNIVERSITY OF TECHNOLOGY

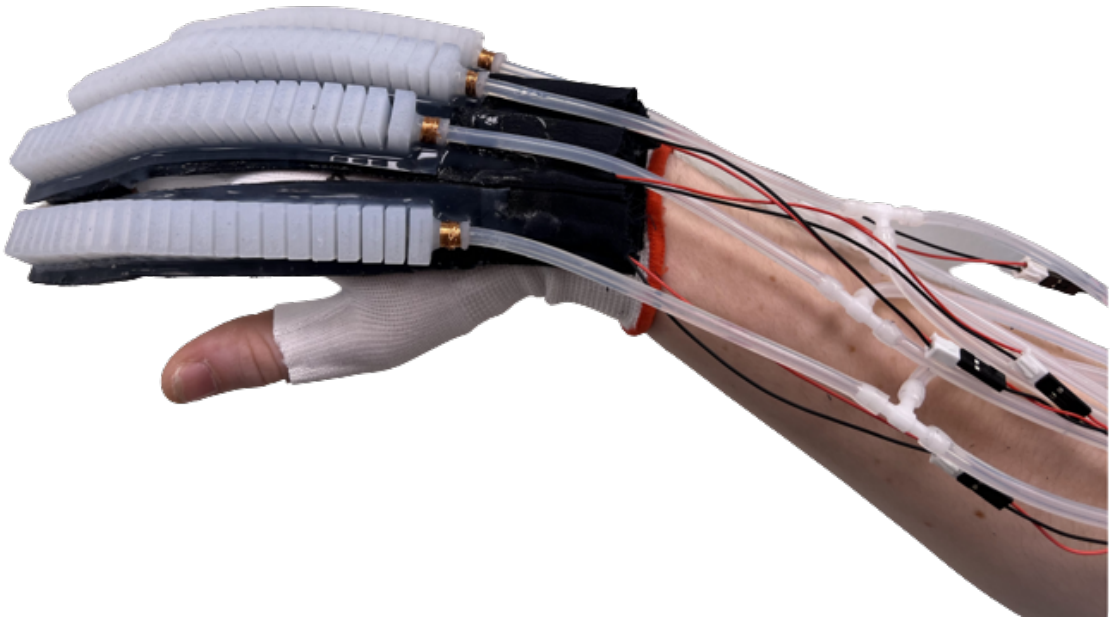

Pneumatic soft robotic glove for hand rehabilitation

Evaluating different types of material and soft actuator designs to construct a prototype of a soft robotic pneumatic glove for hand rehabilitation.

Bachelor's thesis in Automation and Mechatronics

SOFIE ANDERSSON, FELIX GRÅHN, ALEXANDER HEIJKEN-SKJÖLD, ZACHARIAS LIND, SACKARIAS LUNMAN, ANTON STRANDROTH FRID

DEPARTMENT OF ELECTRICAL ENGINEERING
CHALMERS UNIVERSITY OF TECHNOLOGY
Gothenburg, Sweden 2023
www.chalmers.se

Bachelor's thesis 2023

Pneumatic soft robotic glove for hand rehabilitation

Evaluating different types of material and soft actuator designs to construct a prototype of a soft robotic pneumatic glove for hand rehabilitation.

SOFIE ANDERSSON
FELIX GRÅHN
ALEXANDER HEIJKENSKJÖLD
ZACHARIAS LIND
SACKARIAS LUNMAN
ANTON STRANDROTH FRID

CHALMERS
UNIVERSITY OF TECHNOLOGY

Department of Electrical Engineering
Chalmers University of Technology
Gothenburg, Sweden 2023

SOFIE ANDERSSON, FELIX GRÅHN, ALEXANDER HEIJKENSKJÖLD, ZACHARIAS LIND, SACKARIAS LUNMAN, ANTON STRANDROTH FRID

Supervisor: Rikard Karlsson, Department of Electrical Engineering
Examiner: Emmanuel Dean, Department of Electrical Engineering

Bachelor's Thesis 2023
Department of Electrical Engineering
Chalmers University of Technology
SE-412 96 Gothenburg
Sweden
Telephone +46 31 772 1000

Cover: Prototype of a soft robotic pneumatic glove for hand rehabilitation.

Typeset in LaTeX
Gothenburg, Sweden 2023

Pneumatic soft robotic glove for rehabilitation
Evaluating different types of material and soft actuator designs to construct a prototype of a soft robotic pneumatic glove for hand rehabiliation.
SOFIE ANDERSSON, FELIX GRÅHN, ALEXANDER HEIJKENSKJÖLD, ZACHARIAS LIND, SACKARIAS LUNMAN, ANTON STRANDROTH FRID
Department of Electrical Engineering
Chalmers University of Technology

Abstract

The intention of this paper is to add to the knowledge base of Chalmers University of Technology about soft actuators in rehabilitation applications for stroke-induced hand impairment. In this work, a glove was fabricated that can assist a patient in doing common rehabilitation exercises, providing additional finger force.
Evaluating different actuation methods and actuator types based on literature, the most suitable combination to be fitted on a rehabilitation glove was found. The PneuNet and the extending McKibben actuator were manufactured using various silicone stiffnesses, and compared in terms of fingertip force generation and bending angle. The results show that a pneumatic PneuNet with silicone stiffness 20 shore A has superior characteristics, and was hence chosen to be fitted on the rehabilitation device powered by a series of syringe pumps using linear actuators.
A user interface was developed that allows the user to control which motions to perform. Furthermore, a system to approximate the finger joint bending angles was developed, obtained by training a linear regression model on flex resistance, internal pressure and linear actuator position.

Keywords: soft robotics, soft actuators, PneuNet, fiber-reinforced actuator, extending McKibben, stroke rehabilitation glove, pneumatic supply system, syringe pump, fingertip force

Sammandrag

Avsikten med detta projekt är att bidra till Chalmers tekniska högskolas kunskapsbas om användningen av mjuka aktuatorer för rehabilitering, mer specifikt strokerelaterad nedsättning av handfunktion. I detta arbete tillverkades en prototyp av en handske som kan hjälpa en patient att göra vanliga rehabiliteringsövningar genom att tillföra en yttre kraft. Genom att utvärdera olika aktueringsmetoder bedömdes de pneumatiska aktuatorerna vara lämpligast; därav jämfördes två olika typer av mjuka pneumatiska aktuatorer (PneuNet och den förlängande McKibben-aktuatorn). PneuNet- och den förlängande McKibben-aktuatorn tillverkades i silikon med olika styvhet och evaluerades genom mätning av den maximala kraften genererad från fingerspetsen samt deras rörelseomfång i varje led. Resultatet visar att PneuNet tillverkad i silikon 20 shore A har de bästa egenskaperna för projektets syfte, och valdes därför till att monteras på prototypen. Det pneumatiska drivsystemet som används för att trycksätta aktuatorerna består av en serie av sprutor som drivs med hjälp av eldrivna linjära aktuatorer. Ett användargränssnitt utvecklades för att på ett enkelt sätt låta användare styra vilka rörelser som ska utföras. Vidare utvecklades ett system som med hjälp av en linjär regressionsmodell kan approximera fingrarnas totala böjningsvinklar utifrån flexmotstånd, inre tryck och position på den linjära aktuatorn.

Acknowledgements

This endeavor would not have been possible without our supervisor Rikard Karlsson and our examiner Emmanuel Dean, who have given us their support throughout the whole process and shared with us their knowledge in the field to help us finalize our prototype.

Contents

List of Figures

List of Tables

1

Introduction

According to the World Stroke Foundation, approximately 12.2 million people are affected by stroke every year [1]. In Sweden, it is the most common cause of long-term disabilities for adults [2]. The damage caused by a stroke depends on which part of the brain is affected, and how widespread the damage is [3]. One of the most common complications observed is loss of hand and finger function, which can be seen in up to 75% of those affected [4]. This kind of disability often affects the patient's ability to do simple tasks such as cooking, dressing, or picking up items. It affects the ability to participate in activities of daily life (ADL), leading to impaired quality of life [5].

Some disabilities are permanent and the patient will have to adapt to the new circumstances, but in many cases, it is possible to improve the function of the affected body part with proper rehabilitation [3]. Looking specifically at the motor function of the hand, high-intensity training (>3 h/day, 5 days/week during 10 weeks) with task-specific movements that the patient will need to participate in everyday life, is shown to give the best result [6]. The ability to grasp or pinch objects is crucial for ADL, and can therefore be seen in many of the commercial hand rehabilitation programs focusing on regaining the functionality of the hand [7], [8]. The training is often performed both independently by the patient, but also with support from a physiotherapist, to ensure that a high amount of training is achieved [6]. This rehabilitation process can be slow, stressful, and frustrating for the patient, as well as labor-intensive and time-consuming for the physiotherapist [9].

1.1 Background

To enhance the rehabilitation process for stroke patients, various tools can be employed to empower patients to perform rehabilitation exercises independently, without the direct aid of a physiotherapist. One tool that has traditionally been used is a rigid exoskeleton-based hand rehabilitation device which has been shown to significantly improve hand functions in chronic stroke patients [10]. Another tool that is used for post-stroke rehabilitation is a soft actuator-based hand rehabilitation device. Soft actuators have been increasingly used in rehabilitation in recent years and there is an increasing trend in the development of soft actuators [11].

Soft actuators have many advantages compared to their rigid counterpart. By using

materials with similar stiffness to biological materials and human tissue, it is possible to perform a wide range of complex motions with high flexibility that are not possible using rigid parts. These characteristics could be very useful when developing products to be used by patients in rehabilitation since they are safe to use and could mimic human movements [11]. This could contribute to a better rehabilitation process for the patient and a reduced workload for the physiotherapist.

1.2 Purpose

The purpose of this project is to contribute to the development of soft actuator-based hand rehabilitation devices on Chalmers University of Technology that can improve the rehabilitation process for stroke patients, enhance their quality of life, and reduce the workload of physiotherapists. Furthermore, this project aims to investigate the suitability of different soft actuators for hand rehabilitation purposes, as well as the performance of the most appropriate ones. By evaluating the characteristics of said actuators, this paper can serve as a guide for others when developing soft hand rehabilitation devices.

1.3 Goal

To be able to create a hand rehabilitation device that fulfills its purpose, a suitable soft actuator has to be found and used. The actuators will have to fit onto a glove and also be controlled by the user. The goal of this project can be summarized with the following points:

- Compare several types of soft actuators and identify the most suitable soft actuator type for this project.
- Analyze various designs of the chosen soft actuator type to determine the optimal design for this project.
- Use the optimal soft actuator to create a glove that could be used for hand rehabilitation that is able to perform one common hand rehabilitation motion (grasping).
- Implement individual control of each soft actuator, thus enabling the rehabilitation exercise finger opposition (further described in Sec. 3.2).
- Design a predictive model that can estimate the bending angle of the optimal soft actuator design, to lay the groundwork for closed-loop feedback in future projects.
- Implement an intuitive and user-friendly control of the soft actuator glove.

1.4 Limitations

There are time and budget limitations set by Chalmers; the maximum cost of the project is restricted and the time frame is 19 weeks. Because of the limited time

for the project and the complexity of hand motions, some limitations are needed to reach the goal. The robotic glove will not include a soft actuator for the thumb. Furthermore, individual finger joint control will not be considered. Hence, during actuation, the fingers will always bend on each joint.

2

Ethics

The two main groups that will be affected by developing the rehabilitation glove are the patients, physiotherapists, and other health care workers using the technology. By observing the interests of each stakeholder both advantages and disadvantages can occur and these must be considered.

This technology could contribute to a more efficient rehabilitation process for patients with reduced hand function [6], [9], [11], [12]. It would give the patient more freedom to work on their rehabilitation in a time and place that matches their own needs, without having to make an appointment with a physiotherapist [9]. With patients able to rehabilitate more independently, the physiotherapist will be able to use their time for other patients that are in greater need or do not have the same ability to work independently. This could result in more patients getting the help they need.

However, other things could be discussed when considering who will be using the glove. Approximately 75% of those affected by stroke are above 65 years old [13]. By providing them with the glove, it is expected that they can use it independently. This could be problematic in some ways. One perspective is that the elderly population is not as used to these kinds of technical aids and does not have the same ability to adapt to new technologies as the younger population [14]. There is also a widespread problem that many elderly people are socially isolated and experience loneliness, which could affect the patient's mental and physical health [15]. Providing them the glove for rehabilitation also means removing social interaction from a patient, since the other option would be to work together with a physiotherapist. The mental and physical health, as well as the experienced overall well-being, of the patient, is just as crucial for the patient's health as other physical factors and should therefore be considered [16].

Regarding this project, the benefits outweigh the downsides. Creating a device that is simple to use and making sure the patient is well informed will decrease the risk of the patient not being able to handle the product, and by being aware of the patient's social health, problems regarding decreased social interaction can be considered.

3

Theory on Soft Actuator-Based Hand Rehabilitation

To be able to construct a rehabilitation glove, information from different fields is needed, including the anatomy of the human hand, soft actuators, and software for control and performance measuring. This report is reviewing some examples of actuation methods, designs and different materials for the soft actuators, as well as different control systems and the usage of surface electromyography (sEMG).

3.1 The Anatomy of the Human Hand

The human hand is built up by a complex network of bones and muscles, making it possible to perform a wide range of motions with high precision [17] and with over 25 degrees of freedom [18]. The muscles can be divided into two different groups. The extrinsic muscles, originating from the forearm, connect to the hand, while the intrinsic muscles are composed of smaller muscles whose attachment and origin both lie within the hand. The most difficult part of the hand to control is the thumb as it has a lower coordinated relationship compared to the rest of the fingers [18]. It is also shown that the thumb needs to move independently from the other four fingers of the hand to perform various tasks. The four fingers of the hand have three bones (distal, middle and proximal phalanx) and three joints (interphalangeal joint (PIP), metacarpophalangeal (MCP) and distal interphalangeal (DIP) joints). However, the thumb only has two bones (distal and proximal phalanx) and two joints (interphalangeal (IP) and MCP joint) [19]. An illustration of the human hand with all the joints displayed can be seen in Fig. 3.1.

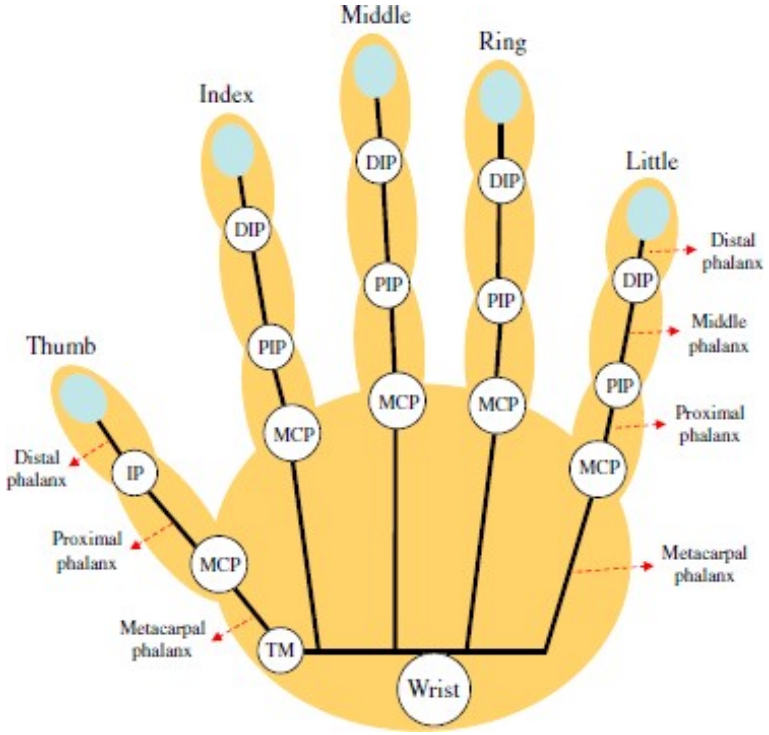

Figure 3.1: Anatomy of the hand, from [19] © *2014, IEEE*.

3.2 Hand Rehabilitation

With physiotherapy, many of those affected by stroke can improve their hand function. Studies show strong evidence that highly repetitive task-oriented and task-specific training is the most efficient rehabilitation [6]. The ability to grasp or pinch objects is crucial for ADL, and can therefore be seen in many of the commercial hand rehabilitation programs focusing on regaining the functionality of the hand [7], [8]. There are also studies showing the importance of being able to help the patient open and close their hand, and that this could be done efficiently with soft robotics helping the patient[12].

The most simple exercise used in rehabilitation is grasping, where the hand should move from open hand to closed fist, performing a full range of motion (Fig. 3.2).

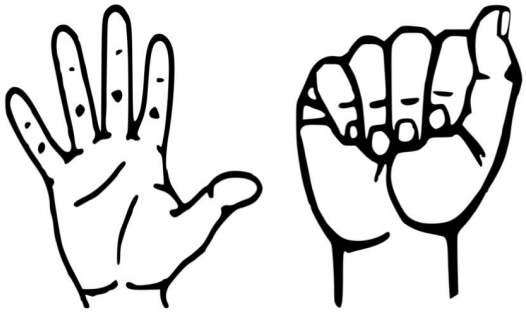

Figure 3.2: Open hand to closed fist, from [20], [21]. Modified with permission.

Another common exercise for post-stroke rehabilitation is finger opposition. The exercise is performed by bringing the tip of the index finger to the tip of the thumb to form a ring, followed by pinching and releasing. The same motion is repeated for middle, ring and little finger [8] (Fig. 3.3).

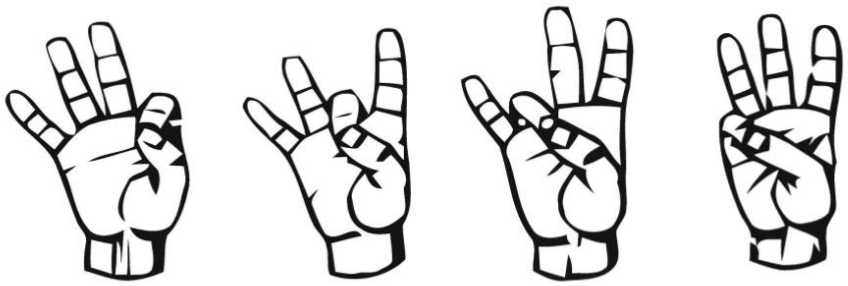

Figure 3.3: Finger opposition, from [22]–[25]. Modified with permission.

To perform ADL, the finger joints need to have a functional range of motion (FROM). Different definitions of FROM occur in related literature. In a study by Bain et al. [26] the FROM of the joints in the hand were measured. The study involved having 10 participants performing 20 different ADL tasks. Bain et al. [26] defined FROM as the range necessary to perform 90% of the activities. In a similar study by Hume et al. [27], the FROM was instead defined as the arc of joint motion needed to accomplish a designated task. However, as Bain et al. [26] point out [26], this study only takes static hand gripping tasks into account and excludes the transport and pre-grasping components of gripping. The FROM of the finger joints, excluding the thumb that are displayed in Tab. 3.1 are based on the study by Bain et al. since their study included these components.

Joint	FROM (°)
MCP all	52
PIP all	64
DIP all	54

Table 3.1: Functional range of motion (FROM) of the joints in the hand, including the Standard Deviation (SD).

In order to perform different ADL tasks, it is essential to not only consider the bending angle of each joint but also to acquire the specific fingertip force required. The actual fingertip force to achieve ADL varies between different publications. Smaby et al. [28] used a robot arm with a force sensor to determine the force requirement for some common ADL tasks such as inserting a card into an ATM and using a fork. To complete 9 out of 12 of these tasks, 10.5 N was required. Polygerinos et al. [9] determined that for their soft robotic glove, each soft actuator would need to excert 7.3 N in fingertip force. In contrast, Wang et al. [29] estimated the range of daily activities and determined that 20 N in fingertip force would be required.

3.3 Existing Solutions for Soft Actuators

When examining literature about soft actuators, there is no strict definition of what conditions are needed to be met in order to classify as a soft actuator. One common interpretation implicates is that they are made out of compliant materials and have no fixed degree of freedom. Li et al. [30] describes said field of robotics in the following way: "Inspired by physically adaptive, agile, reconfigurable and multifunctional soft-bodied animals and human muscles, soft actuators have been developed for a variety of applications, including soft grippers, artificial muscles, wearables, haptic devices and medical devices". This section presents existing solutions for soft actuators. The three categories that will be described are fluidic actuators, electric actuators, and tendon wire-driven actuators.

3.3.1 Fluidic Soft Actuators

Fluid-driven soft actuators utilize pneumatic or hydraulic pressurization of a fluid inside a hollow soft body [31]. The overpressure induces force and subsequently deformation of a soft structure. There are various ways in which deformation in response to a pressure increase can be achieved, with different advantages respectively. The purely expanding motion caused by exposure to internal pressurization constitutes the basis for achieving diverse types of deformation of a more complex nature. Soft actuators are well suited for these types of applications because of their compliant nature, compared to traditional, strictly mechanical structures [31].

Although possessing several beneficial properties, fluidic actuators require certain equipment such as compressors/pumps, valves, and pipes which can be bulky. Other drawbacks include potential leakage leading to loss of power, and the need for advanced control systems to achieve precise positioning with decent repeatability [32].

One well-recognized actuator is the McKibben actuator. It consists of an inflatable bladder surrounded by an external double helical weave acting as a constraint that contracts as it is being expanded radially [33]. As the fluid pressure increases inside the bladder, it expands radially, giving rise to longitudinal contraction of the surrounding weave. As a result, the artificial muscle's length contracts due to the increase in pressure. However, if the bladder is constrained in its radial direction, an increase in internal pressure can give rise to longitudinal expansion instead. By mounting e.g. a spring around the elastic tube, the tube will only elongate since its diameter will remain the same during expansion [34]. This type of actuator is often referred to as 'fiber-reinforced actuator' or 'extending McKibben actuator'. In this report, it will be referred to as any of said terms, or just 'McKibben'.

An alternative design of a soft fluidic actuator implements a bellows-shaped structure. Similar to the circumferential spring in an extending McKibben actuator, the bellows serve as a means of limiting radial expansion and allowing longitudinal expansion. Hence, when exerted to an internal over pressure, the body expands longitudinally [35].

The fundamental design of an elongative actuator, such as the one previously mentioned, can be modified to create bending. To transform a purely extending motion, into e.g. a bending motion, a constraint can be introduced. The constraint's purpose is to make the rigidity of the structure anisotropic, thus causing the structure to bend as it expands [36]. By introducing a strain-limiting fiber on one side, the elongation of the artificial muscle is limited, forcing the structure to bend [36]. Bending motion is particularly relevant for this project as the gripping movement of a human finger is similar to bending, and is desired to be mimicked by the rehabilitation device subject to development. The working principle of a strain-limited bending soft actuator is visualized in Fig. 3.4.

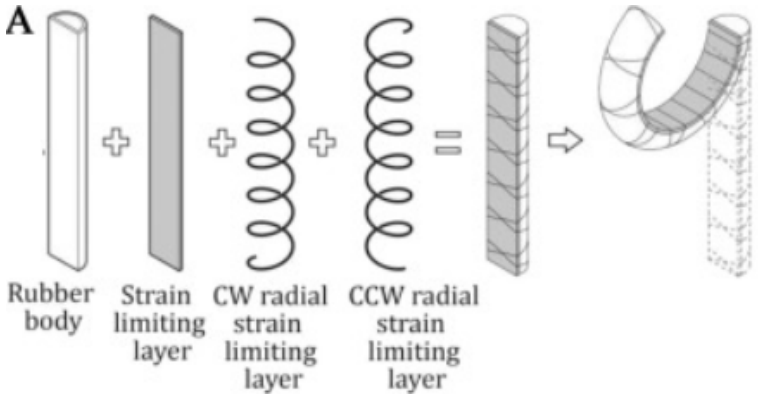

Figure 3.4: Strain constrained extending McKibben actuator, from [9].

Instead of inducing one singular motion of the entire actuator, there are possibilities to create several types of movement throughout a single body utilizing multi-segment actuators [9]. For example, by implementing several segments of fiber-reinforcement, bending focused on only a few instances throughout the actuator can be achieved [37].

Another concept is the PneuNet actuator, which is recognizable by its multiple connected chambers. When it is internally pressurized the chambers inflate, making the actuator expand. A strain-constraining layer is often added to the bottom layer, thus enabling the actuator to bend [38]. Increased tensile stiffness can also be achieved by using a thicker layer of silicone [39]. The bending of a PneuNet actuator can be seen in Fig. 3.5. Another design aspect of a PneuNet soft actuator is the depth of the gaps between the chambers (Fig. 3.6). Chen et al. [38] simulated different depths of the gaps and stated that the thickness directly affects the deformation.

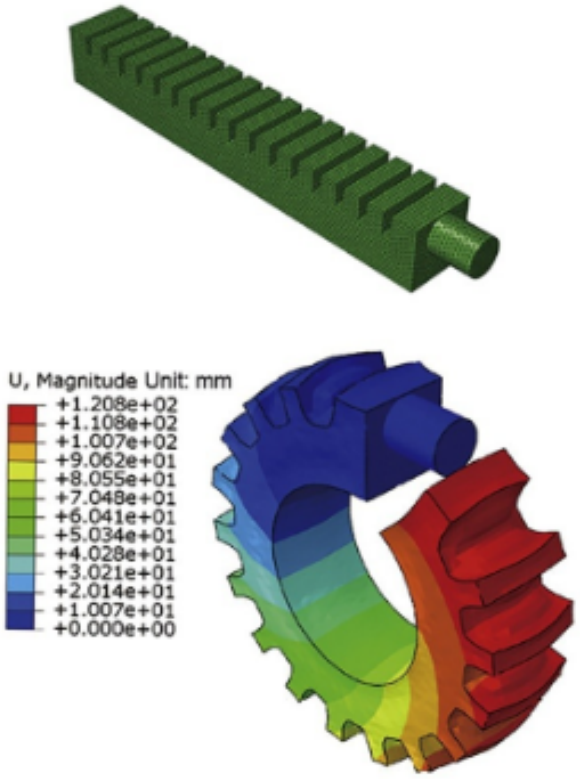

Figure 3.5: PneuNet actuator, from [39].

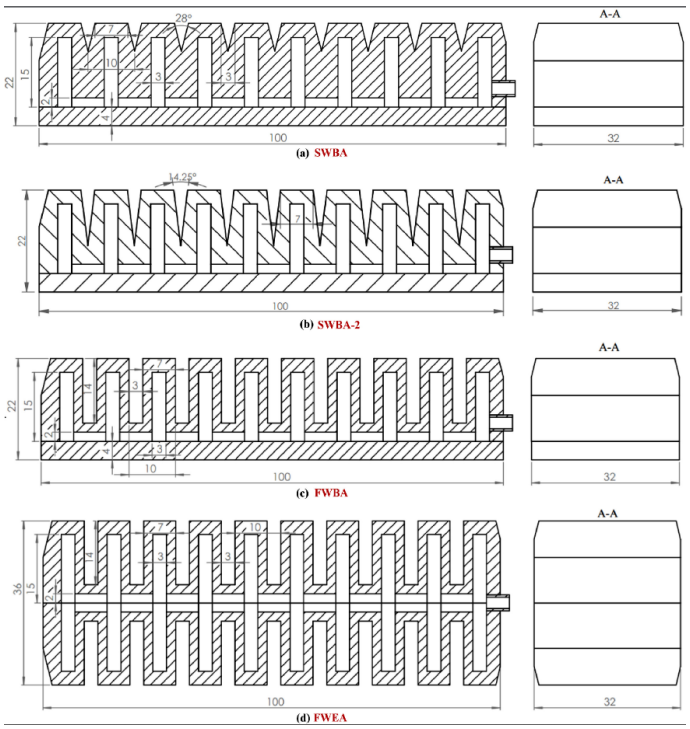

Figure 3.6: PneuNet actuator with different thicknesses, from [38].

3.3.2 Material for Fluidic Soft Actuators

Selecting the appropriate material for a pneumatic soft actuator requires careful consideration of several factors. Firstly, a deformable and elastic material is necessary for the soft actuator to function properly. Furthermore, when developing rehabilitation devices, ensuring safe human-machine interaction is a critical requirement. Choosing a material with elasticity similar to that of human skin can be advantageous in this regard [40]. Many materials are potentially viable for use in soft robotic rehabilitation, but the best choice depends on its impact on two main areas: torque generation and the bending angle of the actuator during pressurization [41]. Additionally, the material must, in combination with the soft actuator design, enable the required motion for hand rehabilitation [42]. Thus, the material selection process involves careful consideration of various factors to ensure the optimal performance of the pneumatic soft actuator.

Gariya et al. [43] compared three different materials for a PneuNet actuator in their work: Elastosil M4601, Dragon Skin 30, and Smooth-Sil 950. The comparison was made using Finite Element Method (FEM) and the obtained result was that for an internal pressure of 20 kPa, Dragon Skin 30 had the highest bending angle (47.5 degrees). Dragon Skin 30 was also subjected to the least stress in comparison to the other two materials.

3.3.3 Electric Soft Actuators

In addition to traditional fluid actuators, there are so-called Hydraulically Amplified Self-healing Electrostatic actuators (HASEL). They utilize voltage fields between two electrodes to induce displacement of a dielectric fluid contained within a soft elastomeric material, causing the structure to swell [44].

Another type of DiElectric Actuator (DEA) consists of two soft electrodes placed on each side of a soft elastomeric layer. Due to attracting Coulombic forces acting on the opposed electrodes when high voltage is being applied, a squeezing force on the middle layer is exerted [45]. As a result of the elastic nature of the mentioned layer, a strain is induced perpendicular to the force direction. In other words, the shape of the actuator is altered allowing it to be implemented similarly to a human muscle in soft robotics applications. For a better view of the working principle of a DEA, see Fig. 3.7.

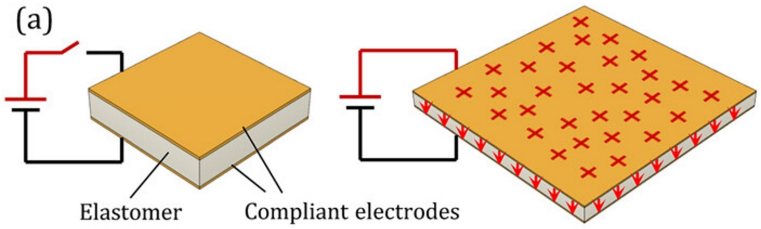

Figure 3.7: Functional principle of a DEA, which flattens when voltage is applied, from [45].

Drawbacks of implementing these technologies for this specific project include the fact that they currently operate at high voltages, in the order of kilovolts [45] [46], which may be problematic when used in the vicinity of humans due to the risk of electrical shocking.

3.3.4 Tendon Wire-Driven Soft Actuators

Tendon wire-driven soft actuators are based on contraction/retraction of tendon wires. Being fastened on one end of a soft body, the contraction/retraction of the tendon wires can give rise to bending of the structure. Similar to other soft actuators, the actuator consists of a tube(s), but instead of keeping fluid, they enable the tendon wires to run freely.

There are different ways of contracting/retracting the tendon wire. The first and possibly least complicated one is by having a pulley system that pulls the tendon wire and thus bends a compliant structure. In many cases, the pulley system often consists of an electric motor that spins a wheel to which the wire is attached. Embedding torsion springs into the structure that is to be deformed, the body can be returned to its initial state as the pulling force is released (Fig. 3.8 and Fig. 3.9) [47], [48]. Instead of retracting the tendon wire, the wire itself can be contracted using a shape memory alloy (SMA) wire, commonly consisting out of Ni-Ti (Nitinol) alloys [49], [50]. When a current is applied to the SMA wire, its temperature increases which causes it to contract. When the current is removed the temperature decreases, and the wire returns to its initial state [49]–[51].

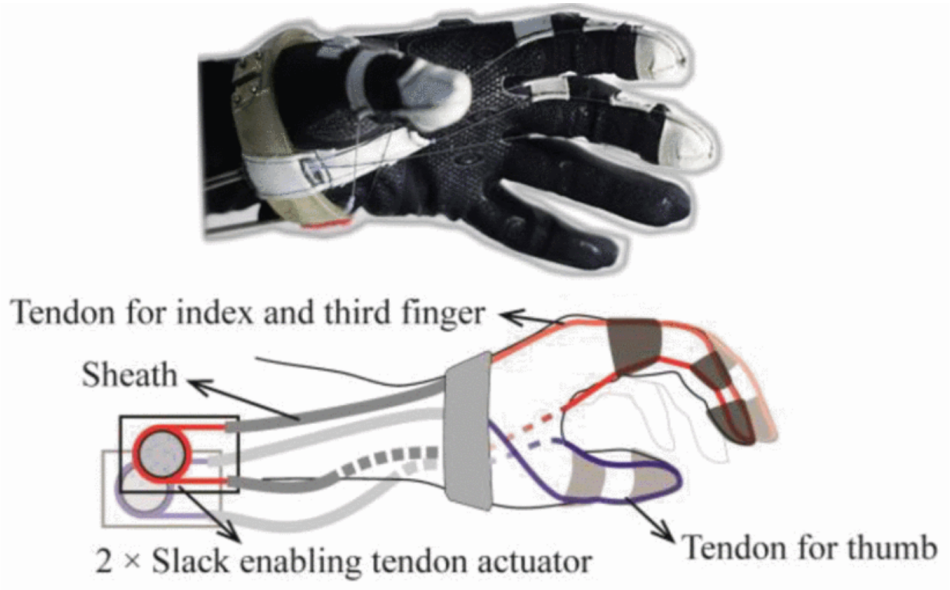

Figure 3.8: Tendon wire-driven actuator using pulley system, from [48] © *2015, IEEE.*

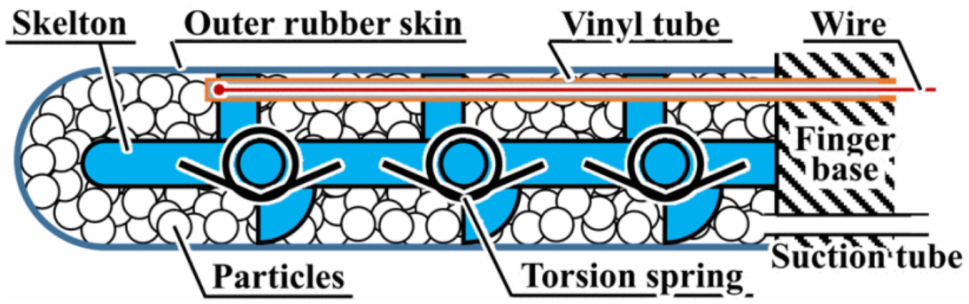

Figure 3.9: Tendon wire-driven actuator with embedded torsion springs, from [47] © *2018, IEEE*.

Kim et al. [49] developed a soft robotic hand and produced various interesting diagrams regarding the performance of the SMA tendon wire-driven actuator during different conditions. The fastest time to reach the maximum deformation (closed fist) was 5.1 seconds. The soft robotic hand was able to grasp various objects successfully. Yin et al. [50] studied the grasping force of SMA wires with different stiffness. The grasping force was measured by a force sensor at an offset from the finger's root. The maximum grasping force obtained in their experiment was 0.676 N with one finger and an offset of 30 mm. Lee et al. [51] measured the tip force of SMA wires of different thickness and diameters of 3 mm, 5 mm, and 8 mm, as well as different length of the wires: 0 mm, 50 mm, 100 mm, and 200 mm. The maximum tip force obtained by the 100 mm SMA wire was almost 0.6 N.

The main benefit of using a tendon wire-driven actuator is that no additional components such as compressors, pumps, and valves are required, which makes the system less complex [49]–[51]. Eliminating the additional components causes a decreased weight as well, which is beneficial when the system is being used or moved. Being powered by electricity directly, the system can maintain a low noise level [50], [51], which is desirable for at-home use. Other benefits include that the actuation method is cheaper compared to the previously mentioned solutions [51].

The main drawback of using an SMA wire-driven actuator is the time it takes to perform the gripping motion and return to the initial state. As mentioned before Kim et al. [49] was able to reach maximum deformation at a time of 5.1 s. The main drawback of using a pulley system to control the actuators is that the internal design is complex as seen in [47], [48].

3.4 Evaluation Methods of Soft Actuator Characteristics

To be able to compare the performance of different actuators, the performance needs to be quantified. In this section, different methods to evaluate the mechanical behaviour of a soft actuator will be presented.

3.4.1 Finite Element Method

One way to simulate and validate the characteristics of an actuator design is to utilize the Finite Element Method (FEM). FEM "is a numerical analysis technique which can be used to obtain approximate solutions to a wide variety of engineering problems." [52]. By discretizing a domain into elements, one can perform numerical calculations of e.g. deformation given certain boundary conditions. There are multiple tools for implementing the FEM on a modeled design. One example is Ansys Mechanical [53]. Ansys Mechanical allows for several types of structural analysis of a CAD model, including fatigue life analysis.

To perform a finite element analysis on hyperelastic materials such as silicone, a model for the material behaviour is required. Polygerinos et al. [32] used a second order Yeoh model to analyze their soft actuator. Experimental data was used to evaluate the material coefficients and the accuracy of the model. Sun et al. [54] used a three-order incompressible Yeoh material model to analytically evaluate soft hoop-reinforced pneumatic actuators.

3.4.2 Experimental Setup

To evaluate the characteristics of soft actuators, different kinds of experimental setups have been developed [32], [54]–[57]. These often capture the force output at the fingertips, curvature, and displacement of the actuators. More robust setups have been used where experiments can be easily repeated [32], [57]. These setups also have the advantage of being able to make multiple simultaneous measurements.

A common way to measure the output force of a soft actuator is to measure the generated force at its distal tip. Polygerinos et al. [32] measured the output force by clamping an actuator in one end, and having the distal in contact with a multi-axis force sensor while pressurizing the actuator. A similar setup, but with top and side constraints, has also been used (Fig. 3.10) [9]. Yap et al. [57] attached one end of a bending actuator to a fixed plate and the other end to a horizontally moving platform. When actuating, the moving plate would exert a horizontal force on a load cell connected to a computer which in turn measures the horizontal force output.

The generated grip force along the length of soft actuators has also been measured. This is important to ensure "that the forces generated do not impede natural finger motions or cause discomfort to the wearer" [56]. The force exerted along a user's finger can be approximated by attaching force sensors on different segments between the soft actuator and a rigid artificial finger [56]. Yap et al. [55] measured the force

output using flexible force sensors that could either be attached to objects being gripped or directly at the palmar side of the glove.

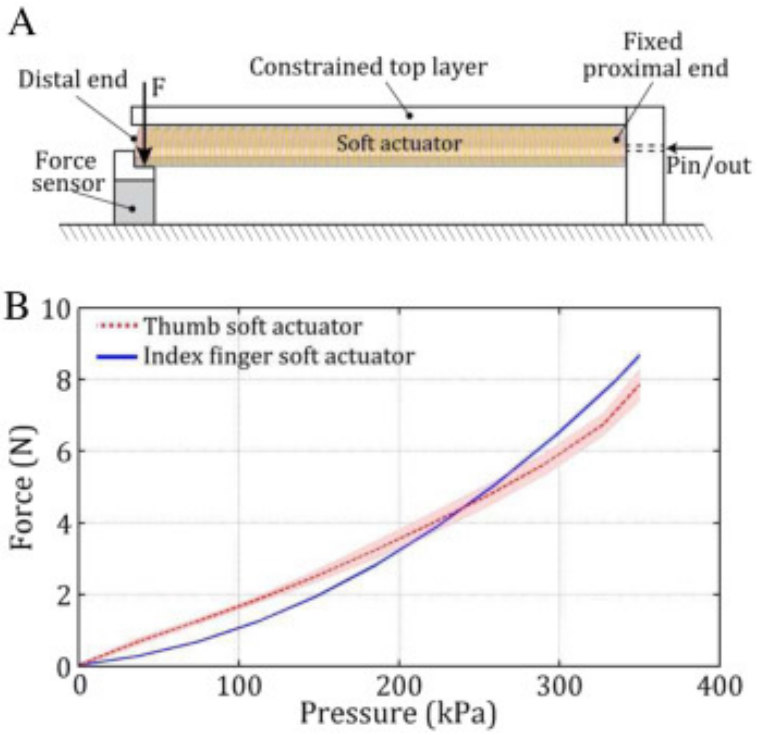

Figure 3.10: Fingertip force experiment setup (A) along with test results (B), from [9].

There are different methods to capture the bending curvature and displacement of the soft actuator. Motion capture systems can be used to evaluate the motion of the actuators and the hand using reflective markers [55], [56]. Polygerinos et al. [32] devised an alternative approach using a high-definition camera to capture the motion of an actuator. They used a checkerboard background and a ruler which served as references to account for distortion and to correlate pixels to length respectively. Another way of measuring the curvature of a soft actuator is to employ an electromagnetic tracking system [9]. To instead measure the horizontal displacement of a bending actuator, a moving plate as presented by Yap et al. [57] could be used.

3.4.3 Empirical Models

Instead of developing analytical models, empirical models can be developed using data-driven analysis. These are often used for highly nonlinear systems when analytical modelling is difficult [58].

Elgeneidy et al. [59] developed empirical models of a soft pneumatic actuator using linear regression and Feed-forward Neural Networks (FNN). Data was gathered using an experimental setup involving a camera, an embedded resistive flex sensor inside the actuator and an onboard pressure sensor. Three linear regression models of the bending angle were developed using the least squares method. Model 1 was trained

on the actuator's flex resistance. Model 2 was trained on the flex resistance and the internal pressure. Model 3 was trained on the flex resistance, internal pressure and initial orientation of the actuator. The best model, model 3, achieved an R^2 score of 0.998, standard error of 1.443°, mean squared error (MSE) of 1.36 and standard deviation (SD) of 1.15. "The R2 value reflects how much of the variance was successfully represented by the model, while the standard error is a measure of the accuracy of the predictions made by the regression model" [59]. The FNN consisted of 1 hidden layer with 7 neurons. It was trained on the same data but achieved a MSE of 0.37 and SD of 0.6 and therefore captured the nonlinearity of the actuator's dynamics better.

Model	**R^2**	**Standard error [deg]**	**MSE [deg^2]**	**SD [deg]**
Model 1	0.880	2.280	4.13	1.94
Model 2	0.943	1.576	1.54	1.21
Model 3	0.998	1.443	1.36	1.15
FNN	-	-	0.37	0.60

Table 3.2: Comparison of the regression and error statistics for three linear regression models and the FNN model.

3.5 Control System

There are many different methods of feedback control for soft actuators [60]. Some successful algorithms are Proportional-Integral-Derivative (PID) controllers and Model Predictive Control (MPC) [61]. Traditional high accuracy feedback control of soft robots has been struggling to optimize performance and increase effectiveness while keeping the robot safe for interactions with humans [60]. An algorithm that has been used to answer this issue is Iterative Learning Control (ILC) which has been combined with the above algorithms to yield good results [61]. ILC can gradually improve the performance of control systems for situations that are repetitive [62], which is well suited for hand rehabilitation exercises.

There are different learning approaches to different controllers. From previous studies, three different learning approaches can be identified: (1) model-based learning, (2) model-free learning, and (3) data-driven learning [58], [61]. Model-based controllers such as MPC are more predictable and accurate than model-free controllers, but they require that the models are accurate to function well. Model-free learning is preferred when the system is highly nonlinear and difficult to model. Proving their stability, however, is difficult and they require a lot of parameter tuning. Data-driven learning such as FNN and other machine learning methods have the benefit of not having to analytically create a model of a given system. Instead, an empirical model is created through data [59]. However, this requires a large amount of data in different operating conditions. Hybrid controllers that combine different control methods have been proposed. Hybrid models often combine a model-based controller, using an analytical model to capture the intrinsic properties of the soft actuator, with a model-free controller to compensate for uncertainties in the dynamics [58].

Balasubramanian et al. [63] proposed combining PID and ILC for angle control using McKibben actuators. The control scheme consisted of an outer loop (OL) controller and an inner loop (IL) controller. The OL controller is a simple open-loop controller that aimed to create a smooth command signal. The IL controller consists of PID controllers for each joint. Three of these joints also have ILC because of their highly nonlinear dynamics which can produce varying responses from linear PID controllers. For the joints using ILC, the final control signal was a weighted combination between the PID controller and ILC. The absolute mean error after four trials was less than 3°.

Elgeneidy et al. [59] developed a PID control scheme based on a data-driven empirical model trained on real-time sensory input from the internal pressure sensor and bending flex sensors. Using both sensors, the controller can adjust for different pressure levels but also compensate for external disturbances. The PID gains were tuned using Ziegler–Nichols method [64] and further tuned manually. When the reference signal was set to a sinusoidal function the MSE was 0.752 and SD was 2.09 with a convergence time of 150 ms.

Sugiyama et al. [61] followed the data-driven approach using an FNN to derive an inverse model of a fiber-reinforced soft bending actuator (FRSBA). The FNN consisted of one hidden layer and was trained on trajectory tracking data from an ILC. The data was low-pass filtered before being used to reduce noise. Four FRSBAs were used to test if the ILC could adapt for each actuator's deformability and were trained for 15 iterations. The Root Mean Squared Error (RMSE) of the trajectory tracking was improved using different conversion functions that reduce the nonlinearity between the step response and the corresponding steady response of the FRSBA.

3.5.1 sEMG Sensor

Surface electromyography (sEMG) sensors can study and record the electric activity of the muscle [65]–[67]. When EMG signals are measured directly from the surface (skin) it is called sEMG, hence the name of the sensor. The amplitude of the signal will depend on how much muscle activity there is, much activity results in high amplitude. The recorded sEMG signal includes not only the muscle activity but also other factors that can impact the signal quality, such as skin and electrode impedance, as well as instrument noise [66]. One well-known device that measures sEMG signals is the Myo Armband from Thalmic Labs, seen to the left in Fig. 3.11. The Myo armband is equipped with 8 EMG sensors, which are used to detect and recognize hand gestures and movements. Additionally, it features a 9-axis inertial measurement unit (IMU), made up of a gyroscope, accelerometer, and magnetometer, that helps to detect arm movements [65]–[67]. To identify which hand gesture is performed by studying the EMG signal, a deep learning model has to be created and trained [65]. The model takes the combination from all sensors as an input and then evaluates which hand gesture is performed. Thalmic labs have developed software for the Myo Armband, called Myo Connect. This enables the user to control slides in a presentation program, online games, etc [68]. There have also been Python

libraries created that enable the user to recognize the hand gestures from the myo armband, one noteworthy example is the PyoMyo library [69].

Another similar sEMG armband to the Myo Armband is the gForce Pro by OYMotion, seen to the rigth in Fig. 3.11, it also consists of 8 surface electrodes and a 9-axis IMU. The main difference is the sampling rate, 1000 Hz for gForce Pro and 200 Hz for the Myo Armband [70]. Both of the armbands are suitable for recognizing hand gestures and therefore also suitable for this project.

Yang Liu et al. [71] present a wearable-based system for tracking 3D hand pose using sEMG from previous mentioned commercial armbands (Myo and gForce Pro). They have managed to achieve real-time tracking of the hand with an error of about 26mm for 14 skeleton joints. They also highlights the primary design challenges in their WR-hand, which are the fixed sensor positions, the twist muscles in the forearm as well as the varying of the wearing position.

Figure 3.11: Myo armband by Thalmic labs and gForce Pro by OYMotion, from [70] © *2021, IEEE*. Modified with permission.

3.6 Computer Vision

To estimate the bending angle of a soft actuator using various input data (such as internal pressure for fluidic actuators), a method of measuring the bending angle is needed. One method is using computer vision. To measure the relative position of an object in a camera frame, fiducial markers can be used. These consist of patterns that are mounted on surfaces and are detected by an accompanying detection algorithm [72]. Some of these markers include: (1) ARTag, (2) ArUco and (3) CCTag. (1) ARTag is one of the most widely used marker types. It uses monochromatic square markers with an internal pattern that encodes the marker with an ID. (2) ArUco markers are similar but can be used for configurable libraries. This allows for smaller custom made libraries which reduces computing time [73]. One of the most popular computer vision libraries OpenCV [74] has an inbuilt module for ArUco detection. (3) CCTag markers differ from the other two in that the markers are concentric black and white rings [73]. This pattern allows for robust detection in blurry conditions.

4

System Design and Development of Soft Actuators

This chapter focuses on the development of soft actuators and the design of the overall system. The requirements for the soft actuators and system design are established to ensure that they meet the desired specifications. Different types of soft actuators, such as electric, tendon wire-driven, and fluidic actuators, are evaluated, considering their advantages and limitations. The pneumatic supply system is dimensioned to meet the requirements, and the selection and implementation of sensors are also presented. Finally, the chosen soft actuator designs are presented, along with the method of prototyping and material choices.

4.1 Requirements

The rehabilitation glove should have properties that satisfy the goals of this project. In this section, the requirements will be motivated and listed, see Tab. 4.1.

The soft actuator should have a sufficient force output. The required fingertip force varies between publications, but the chosen value for this project is 10.5 N since its the median of the three given values. The soft actuator should also achieve full range of motion in the MCP, PIP and DIP joints as specified in Tab. 3.1.

The assistive device should be compatible with a human user. Therefore, the maximum motion speed must be similar to that of the patient. Given that the gripping speed of the patient is impaired, 5 seconds was assessed to be an adequately short time for the soft actuators to perform the full range of motion.

One important requirement is that the weight situated on the patient's arm should not be overwhelming and affect the ability to perform the rehabilitation exercise. Therefore, the maximum weight placed on the arm is set to 0.5 kg.

To facilitate verbal communication between the patient and other people (e.g. a physiotherapist), one should be able to have a conversation during the operation of the device. Hence, the acceptable noise level measured at a distance of 1 m is set to 60 dBA, as it corresponds to that of normal conversation [75].

The device should be safe. Under no circumstances should the glove exert a hazardous magnitude of the force on the user. Neither should it be able to lock in a position where the patient can not remove the glove. Therefore, an emergency stop

will have to be implemented that neutralizes the pressure inside the actuators, thus making the glove removable and secure.

Criteria	Value	Test
Min. force development per finger	>10.5 N	See Sec. 6.1
Full range of motion	Yes	See Sec. 6.1
Max. time to perform full range of motion	<5 s	Manual timing
Max. weight on arm	<0.5 kg	Weighing
Noise level	$\leq$ 60 dBA	Measurement at 1 m distance
Emergency stop	-	Functional test

Table 4.1: Listing of all requirements.

4.2 Determination of Soft Actuator Type and System Design

This section will briefly motivate the choice of the most suitable soft actuator type by comparing the previously presented principles (Sec. 3.3). Furthermore, a decision will be made regarding which of the designs within the chosen actuator type that will be studied further. Additionally, the actuation method, sensor types, and system layout are going to be determined and presented.

4.2.1 Evaluation of Soft Actuator Types

In this section, the soft actuator types presented in Sec. 3.3 are evaluated, including advantages and disadvantages for each one. Finally, a conclusion is drawn regarding which of the types are the most suitable.

Electric Soft Actuators

The main drawback of using electric soft actuators such as HASEL or DEAs in near-human applications is the high voltages required to actuate them. One of the goals of this project is to develop a hand-rehabilitation glove (Sec. 1.3), which will be situated near the skin of the patient when performing exercises. To not run any risk of electrically shocking the patient and thus cause discomfort or potential hazards, electric soft actuators are ruled out as candidates to be implemented in the glove.

Tendon Wire-driven Soft Actuators

Tendon-wire driven soft actuators can be actuated in two ways, either by using an SMA wire or by using a pulley system. From the data provided by Kim et al. [49], it is possible to see that using an SMA wire will be too slow with respect to the requirements of this project. Also, the maximum obtained fingertip force using this method is around 0.6 N [51], which again is too low. A pulley system on the other hand may be fast and forceful, but requires rigid inner parts, and for it to be considered a soft actuator, a soft outer shell has to be applied. Tendon-wire driven

actuators are mentioned as soft actuators in some literature [48], however, we do not regard it as such since the actual force actuation is performed by the rigid parts. Therefore, the tendon-wire driven actuator will not be investigated further.

Fluidic Soft Actuators

The remaining soft actuator type of the ones considered is the fluidic type. Fluidic-type actuators comprise pneumatically and hydraulically driven actuators. The main difference between the two is the actuation medium. Pneumatic systems use a gaseous medium, such as air [11], whilst hydraulic systems use a liquid, such as oil or water [76]. These two methods will be compared in order to choose one of them.

First of all, due to the incompressibility of liquids [77], hydraulically operated systems can deliver a large force using a small displacement volume. Furthermore, position control can be more precise compared to if a compressible medium such as air were to be used [78]. However, due to the higher weight of the actuating medium in a hydraulic system compared to a pneumatic system, the total weight of the actuator may also be increased [79].

Having water as the medium in a hydraulic system may lead to corrosion [80], which in turn can cause leakages. On the contrary, using oil for the medium will prevent corrosion and provide better lubrication [76]. Hydraulic systems are also subject to phenomena called cavitation and aeration. These phenomena can cause damage to the pump and increase the risk of leakages in the long term [79]. By using a pneumatic system, such phenomena do not occur. Another advantage of using a pneumatic system is that air is readily available [80].

With regards to human-centered applications, using oil as the power-delivering medium may be challenging as leakages are hazardous and hard to prevent [81]. A possible solution is to use water as the fluid medium which makes the leakages less hazardous, but still uncomfortable for the user. However, by using air as the fluid medium, the consequences will not be as severe.

In conclusion, using a pneumatic actuation method for a fluidic soft actuator will be the better choice for the application. The inherent safety advantages and reliability of a pneumatic system render it the most suitable option.

Decision of Soft Actuator Designs

Two different types of soft actuators that are commonly mentioned in literature about soft robotics-aided hand rehabilitation have been developed and evaluated, the first being the PneuNet and the second being the extending McKibben. The construction of said actuators differs to a great extent, which is why they were considered interesting to compare.

4.2.2 Evaluation of Pneumatic Supply System

There are different pneumatic supply systems that compress air in different ways, which have both advantages and disadvantages. In this section, the different options

for pneumatic supply systems are described and compared.

One way in which overpressure can be attained, is through a compressor system. Such systems contain a compressor together with valves in order to regulate the pressure inside the soft actuator. It is well-used in similar projects with pneumatic soft actuators [82]. It is often used together with a reservoir that can hold a certain volume of compressed air to increase the capacity and minimize changes in pressure when using the system [83].

Another pneumatic supply system that can be seen in similar projects is air pumps [84], [85], where the pump is connected directly to the actuator, since no reservoir is needed. The pumps are small and can easily be carried with the system while using it. In order to control the pressure inside the pneumatic soft actuator, similar to the compressor system, valves are needed.

Alternatively, a motor-driven piston can be used as the pneumatic supply system. It often uses a syringe combined with a linear actuator to control the position of the piston inside the syringe [86]. This makes the control simple and smooth since the position of the linear actuator can be adjusted precisely [86]. The described pressurization method will from here on be referred to as "syringe pump".

For a device situated directly at a person's body (such as a hand rehabilitation glove), safety is of great importance. To ensure that the system is safe, satisfactory control is critical. Additionally, good control provides high repeatability and ensures that the movement of the actuators are accurate. Consequently, the syringe pump is assessed to be the most suitable option for the applications of this project.

4.2.3 Dimensioning of a Syringe Pump

Different papers on soft pneumatic actuators use different operating pressure. However, since the device developed in this project is intended to be used very close to the human skin, too high internal pressures of the soft actuators can not be allowed for safety reasons. Examples of studies testing the performance of soft pneumatic actuators, related to inducing hand movement, use pressures of e.g. 0-1.5, 0-2, 0-3 bar [87]–[89]. The safety regulations stated by the United States Department of Labor for cleaning using compressed air, prohibit pressures over 30 psi (~2.1 bar) [90]. During cleaning, the air may come in direct contact with the skin and is thus comparable to the application of this project. The law will serve as a reference for the maximum allowed pressure within the system. To account for estimation errors when dimensioning the pneumatic system, a pressure of 1.5 bar (150 kPa) is set as the benchmark.

When dimensioning the system, both the linear actuator and the syringe have to be dimensioned. To make sure the supply system could generate the required pressure and speed, some estimations and calculations were made to know what force the linear actuator had to generate. Firstly, the syringe size was determined. Dilibal et al. [91] developed a finger-sized actuator with an approximate volume of 30 ml, which was used as a reference. Not knowing its volume when inflated, a syringe with a plentiful volume of 60 ml [92] was chosen. The radius r, volume V and

cross-sectional area A of the syringe are:

$$r = 0.013 \text{ m}$$

$$V = 6.0 \cdot 10^{-5} \text{ m}^3$$

$$A = r^2 \cdot \pi = 5.3 \cdot 10^{-4} \text{ m}^2$$

To calculate the required force F of the linear actuator the pressure-force equation was used using the benchmark internal pressure P:

$$F = P \cdot A \implies F = 150000 \cdot 5.3 \cdot 10^{-4} = 79.5 \text{ N}$$

The speed and length of the linear actuator were considered as well, since the actuators have to be able to inflate and expand in the time t, stated in Tab. 4.1. Since the volume increases slightly when inflating the soft actuator, the stroke length l of the linear actuator has to be enough to use the full volume of the syringe. The next step is therefore to calculate the required speed v of the linear actuator in order to achieve the project's requirements. This was done by the following equations:

$$l = \frac{V}{A} = \frac{6.0 \cdot 10^{-5}}{5.3 \cdot 10^{-4}} = 0.11 \text{ m}$$

$$v = \frac{l}{t} \implies v = \frac{0.11}{5} = 0.022 \text{ m/s} = 22.0 \text{ mm/s}$$

Considering these parameters, the Actuonix Miniature Electric Linear Actuator [93] with a gear ratio of 35:1 was chosen for the pneumatic supply system. It has a stroke length of 140 mm and can generate a force of 50 N at a speed of 16 mm/s. Although its maximum force is short of the required, the force output was assessed adequately by looking at its load curve (Fig. 4.1). Knowing that the stall current of the actuator is 650 mA (at the maximum voltage of 12 V), the stall force could be approximated to ~100 N by extrapolating the blue line in the current curve. The approximated stall force exceeds the estimated force necessary to obtain 1.5 bar of pressure (friction forces neglected). Furthermore, it does not exceed the maximum pressure allowed, which was verified first by a rough calculation (see equations below) and secondly by physical testing. However, the actuator does not meet the speed requirement, but is still the fastest choice among the Chalmers-associated contractors given the monetary means at hand.

$$P = \frac{F}{A}$$

$$P = \frac{100}{5.3 \cdot 10^{-4}} \approx 1.9 \text{ bar} < 2.1 \text{ bar}$$

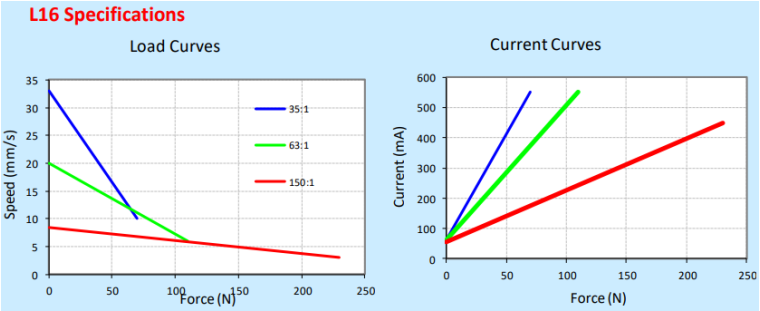

Figure 4.1: Load and current curve of the Actuonix Miniature Electric Linear Actuator, from [93].

4.2.4 Determination of Bending Angle Filter Design

The type of model that will be used to create a filter that can estimate the bending angle of the optimal soft actuator will be empirical and data-driven. The developed models will build upon the research by Elgeneidy et al. [59], specifically the linear regression models. This has the benefits that this project can be compared to theirs and that the models can potentially be further developed using the circumstance that syringe pumps are being used to actuate the soft actuators. This also enables use of flex resistive sensors which are widely used among soft robotic rehabiliation gloves.

The training data will include the measured flex resistance and internal pressure of the soft actuator. The initial orientation is not included since the initial orientation is the same for all experiments. Elgeneidy et al. [59] did not use linear actuators to pressurize their soft actuators. Therefore, the position of the linear actuator controlling the soft actuator is also included in the training data, to evaluate if the models improve using this parameter. The predicted bending angle θ_{bending} is defined as the angle between the line from the CMC to the MCP joint and the line from the MCP joint to the finger tip (Fig. 4.2).

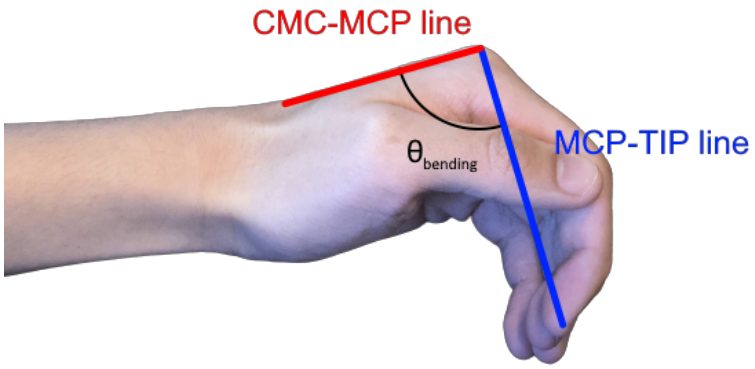

Figure 4.2: θ_{bending} defined by the CMC-MCP line (red) and the MCP-TIP line (blue).

Three linear regression models using the least squares method will be developed for the optimal soft actuator, similarily to Elgeneidy et al. [59]. The first model will only be trained on the flex resistance. The second model will be trained on the flex resistance and the internal pressure. The third one will be trained on the flex resistance, internal pressure and the position of the linear actuator.

4.2.5 Sensors and Electronics

To evaluate and control the soft actuators, information about the actuators needs to be measured by different sensors. A crucial step in this process is to convert the raw sensor readings into meaningful information. In addition to the sensors, there are other electronic components such as the microcontroller that need to be specified.

Force Sensor

To determine the force that the soft actuator exerts, a load cell is used. This kind of sensor converts an applied force into an electrical signal. The advantages of a load cell over, for instance, a resistive force sensor, is that it is highly accurate and is close to linear in its behavior and output. The specific sensor used was an Adafruit 10 kg Strain Gauge Load Cell.

To be able to get a reading from the load cell, a SparkFun HX711 amplifier circuit was used (SEN-13879). In the software, the HX711 library [94] was used. Using the example calibration code from the library, the sensor was calibrated in the software by applying a known force on the load cell. The slope of the output signal was then adjusted until the force reading matched the applied force.

To verify that the load cell is accurate in the force ranges of the developed soft actuators, a verification experiment was run. The load cell was screwed in place on top of a stiff acrylic sheet. Using a SAUTER Manual Wheel Test Stand (TVL-BA-e-1612), forces in the range of 0.2 to 25 N were applied on the load cell.

In Fig. 4.3, the applied force from the test stand is presented on the x-axis and the measured force from the load cell is presented on the y-axis. As can be seen in the linear regression of the applied force against the measured force, the R^2 value is approximated to be 0.9999. This indicates a strong linearity between applied and measured force, thus proving that the result from the load cell can be trusted with a high degree of confidence.

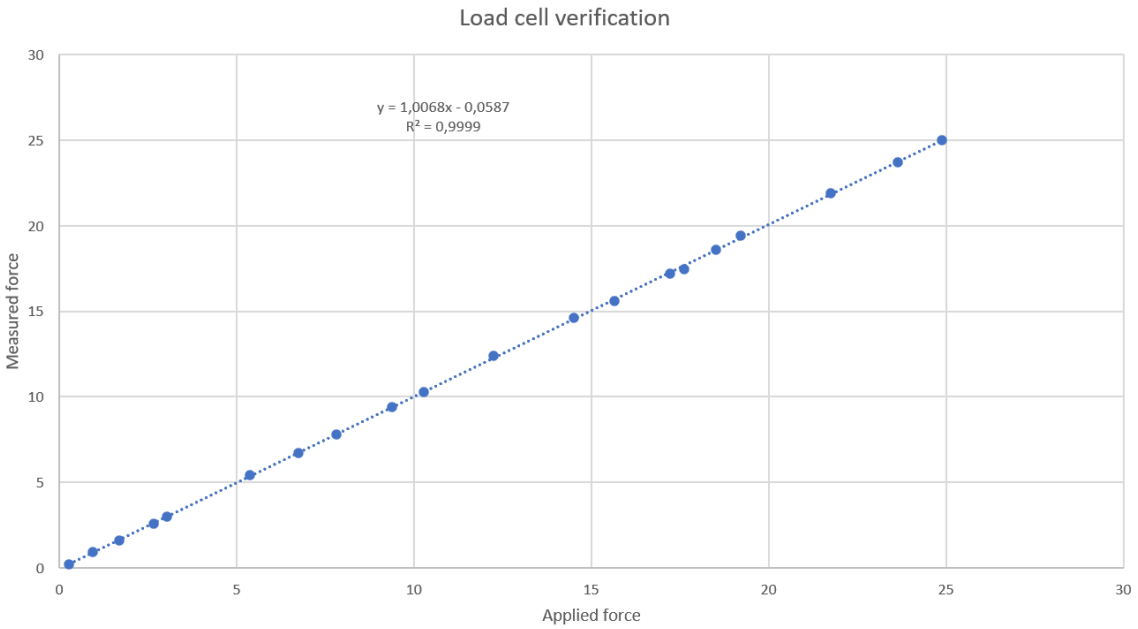

Figure 4.3: Visualisation of correlation between applied force and the measured load cell force.

Pressure Sensor

A pressure sensor can be used to measure the internal pressure of a soft pneumatic actuator. The sensor that will be used is the Honeywell ABP series Basic Board Mount Pressure Sensor (ABPDANV150PGSA3). It can measure pressures between 0 and 150 psi (0–10.3 bar), which in the range of what the syringe pumps will be able to achieve. The pressure can be read using SPI communication, which is simplified using the Honeywell TruStability SPI library [95]. To verify that this library works, the sensor was connected to a compressor with a pressure gauge and the pressure was set to different values. This experiment confirmed that the pressure sensor measures the same values as the pressure gauge.

Flex Sensor

To accurately estimate the bending angle, the empirical model can not rely only on the internal pressure. The bending angle could be influenced by external loads, pressure leakages, etc. To compensate for these discrepancies, a flex sensor is used. The specific flex sensor used is the Spectra Symbol Flex Sensor (SEN-08606) which is a resistive sensor. The sensor has a flat resistance of 10 kΩ when not flexing, and increases in resistance when flexing. Using a simple voltage divider circuit, the voltage over the resistive sensor can be measured using an analog input on a microcontroller.

Motor Controller

The linear actuator used for this project can be controlled in the same manner as a DC motor using a DC motor controller. The speed is controlled using a pulse width-

modulated (PWM) signal from the microcontroller. Taking the maximum voltage and stall current into account, the Adafruit DC/Stepper Motor Driver (TB6612 1.2A) was chosen. The driver can run two linear actuators with a maximum current of 1.2 A for each actuator. Therefore, to run four linear actuators, two DC motor drivers are acquired.

Microcontroller

The sensors, DC motor drivers and other electronic components need to be connected to a microcontroller. The requirements for the microcontroller, based on the needed electronics, are that it can communicate with a PC via serial to communicate with a user and sample data. It should also have pins for 3.3 V and 5 V to allow for sensors that operate using these voltage levels and have enough General-Purpose Input/Output (GPIO) pins for all electronic components. Therefore, the Arduino Mega (Mega 2560 Rev 3) was chosen since it meets all of these requirements and has a plentitude of GPIO pins.

4.2.6 Complete System Design

The complete system comprises of four fingers and four sets of linear actuators, pressure sensors and flex sensors. The four linear actuators will be controlled by two DC motor controllers. The components used for control of the linear actuators and housing of the pressure sensors are contained and soldered on separate prototype boards. This is to make the integration and future troubleshooting easier. An overview of the different modules and their connections can be seen in Fig. 4.4 and Fig. 4.5.

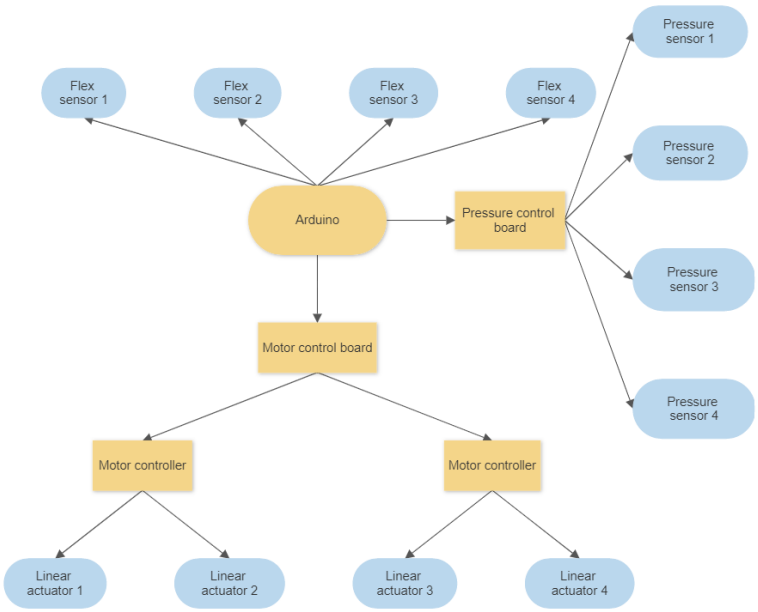

Figure 4.4: Flowchart of the electronic components.

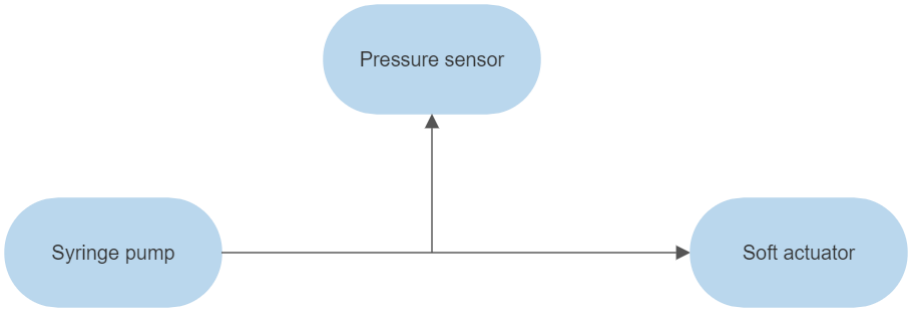

Figure 4.5: Flowchart of the pneumatics of each syringe pump.

4.3 Design of the Soft Actuators

A Computer-Aided Design (CAD) program was used to the design the soft actuators. The program of choice was CATIA V5 as the members of the project had experience with the software. Below, the finished design of each will be described, along with brief descriptions of prior iterations that led up to the final versions.

4.3.1 PneuNet

The design of the PneuNet soft actuator can be seen in Fig. 4.6, and a drawing can be seen in Fig. 4.7. The dimensions were determined to fit onto a human finger. However, the length of the soft actuator mounted on the little finger will be 110 mm instead of 140 mm. The distance between each chamber was inspired by Liu et al. [96]. They showed that the maximum bending angle of the soft actuator could be obtained by using a distance of 1 mm between the chambers. When choosing the wall-thickness of the chambers, it is important to ensure that, when the chamber expands, the walls will squeeze each other and thus make the bending angle increase [96], [97]. Therefore, the wall thickness was chosen to be 2 mm. The design also emphasizes a strong hose connection through the great material thickness and the durable connection to the main body. The thin bottom layer in Fig. 4.6 resembles the impregnated inelastic fabric that is used to prevent the bottom of the actuator from elongating, thus bending the soft actuator. The air tunnel in the bottom has a width of 2 mm in order to prevent the bottom from expanding downwards. When instead using a air tunnel as wide as the actuator itself, the bottom will expand downwards which can be seen in Fig. 4.8.

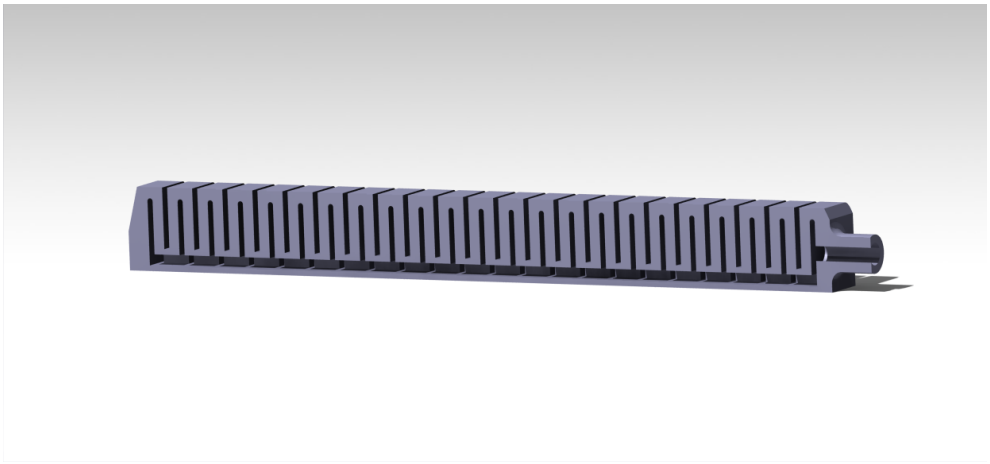

Figure 4.6: PneuNet design.

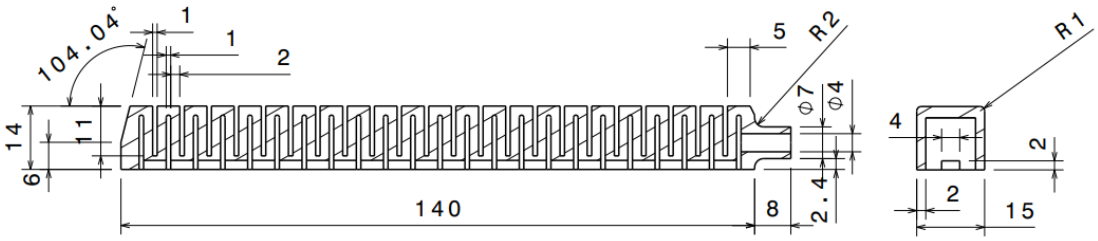

Figure 4.7: Drawing of the PneuNet design.

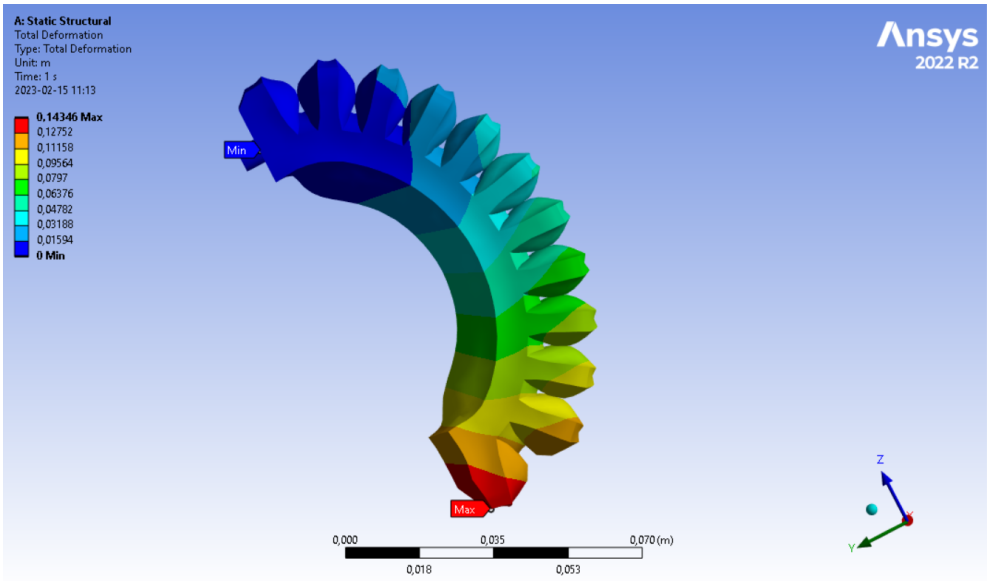

Figure 4.8: Bottom layer expanding downwards.

4.3.2 McKibben

The design that ultimately was chosen to be tested and compared against the PneuNet, was a version much similar to the one presented by Polygerinos et al. [9]. It comprises a rubber hose that has integrated threads, serving as guides for copper wires that constrain radial expansion during inflation. The copper wires run both clockwise and counterclockwise to prevent twisting. The wiring is covered by another layer of silicone that holds the wires in place. The ends are capped with 3D printed parts that are sealed with a silicone adhesive and firmly fastened with copper wire. An inextensible piece of fabric is situated at the bottom, giving rise to a bending motion during actuation.

Although using other cross sectional shapes provide higher bending torque, the hemicircular shape gives the best total bending torque when also considering the bending resistance [98]. On that basis, the hemicircular shape was chosen for the actuator. The outer radius was set to 7.5 mm, which was assessed to be the maximum allowed in order for the actuator to be fitted on a human finger without excessively compromising the hand movement. Despite having a 6.7 mm winding pitch may be considered optimal [99], the pitch of the prototype was decreased to 5 mm to also allow for testing soft silicone mixtures with high pressure. To give the FROM displayed in Tab. 3.1, a cumulative bending angle for all joints of 170° would be required. Polygerinos et al. [98] provided graphs of analytically calculated bending angle as a function of wall thickness and pressure for a soft fiber-reinforced actuator (extending McKibben). Having a wall thickness of 2 mm would result in a bending angle of just above 180° which is in the vicinity of the required FROM. The thickness of the rubber hose was therefore set to 2 mm. The prototype, along with a basic drawing of the rubber hose is displayed in Fig. 4.9 and Fig. 4.10 respectively.

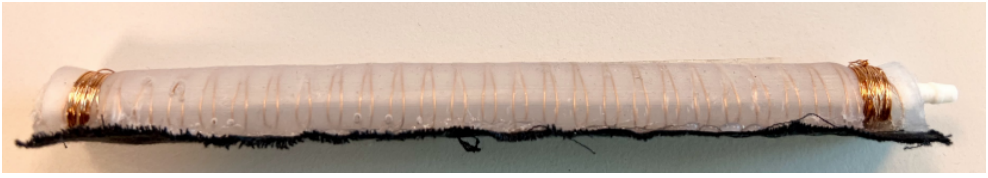

Figure 4.9: Prototype of a McKibben actuator.

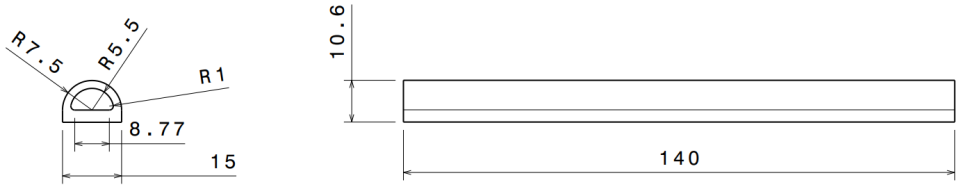

Figure 4.10: Basic drawing of McKibben rubber hose.

4.4 Method of Prototyping for the Soft Actuators

To manufacture the soft actuators, a negative mold was created using the designs of the soft actuators. The molds were then refined by incorporating additional parts into the negative mold, and finally, the molds were 3D printed by a Fused Deposition Modeling (FDM) printer. The soft actuators were then cast by pouring silicone into to the molds and letting it cure.

To make the extraction of the cured silicone out of the molds easier, the molds were treated with a release agent (Ease Release™ 200 spray [100]). This prevented the silicone from sticking to the molds, making it easier to extract. The release agent was applied to both the PneuNet and McKibben molds.

To prevent the captivation of air bubbles within the silicone, it was placed in a vacuum chamber. This process allowed the air pressure to be reduced within the chamber, thereby eliminating the air pockets that would otherwise form within the silicone during the curing process. By removing these air bubbles, the quality and integrity of the final actuator were improved, ensuring that it would be homogeneous and thus more durable and consistent. The process of putting the silicone in the vacuum chamber was done both directly after it was mixed and also after it was poured into the mold. In the second iteration, when the silicone is in the mold, the air bubbles tend to push the silicone out of the mold, leading to the silicone leaking out of the mold. Therefore, a reservoir was created on top of the mold, enabling the silicone to return to the mold. However, the silicone used in this project had a high viscosity, making the air bubbles not disappear as the air bubbles had trouble traveling through the silicone. To solve this issue, a thinner fluid (Silicone Thinner ™[101]) was added to reduce the viscosity level and facilitate the operation. The addition of a reservoir applies to both the PneuNet and the McKibben molds and can be seen in Fig. 4.11 and Fig. 4.12.

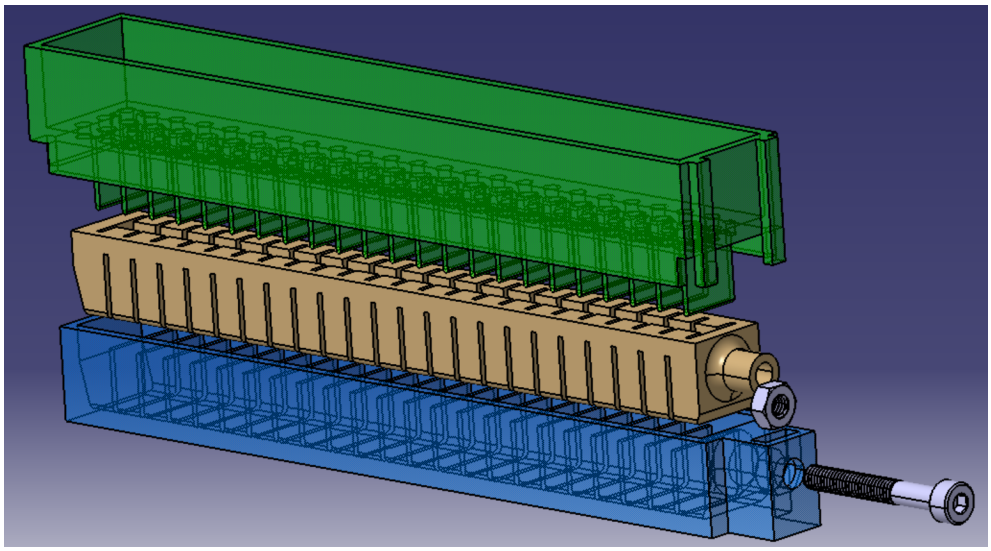

Figure 4.11: The final design of the PneuNet mold is illustrated in this exploded view, with the green-colored top mold, blue-colored bottom mold, and beige-colored soft actuator all clearly displayed.

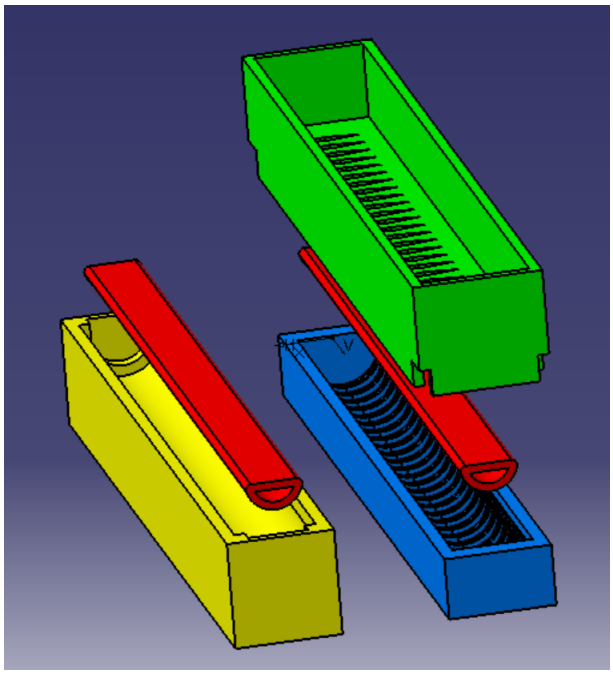

Figure 4.12: The final design of the McKibben mold is illustrated in this exploded view, with the green-colored top mold, blue-colored bottom mold, yellow-colored sealing mold and red-colored core all clearly displayed.

In order to keep the two mold halves aligned, ridges were added to the outer edges of the top mold. However, no ridges were added in the corners since the FDM printer can not print perfect 90° corners. Having ridges in the corners made the parts not align properly and post processes such as filing or grinding were necessary.

A nozzle was included in the PneuNet mold to make a protruding hose connection. The centered hole in the nozzle is achieved by using an M4 nut and screw. The nut is inserted in the pocket seen in the bottom right in Fig. 4.11, and is later glued in place. The screw is then screwed into place through the nut.

4.4.1 Casting Process Step by Step - PneuNet

The following section describes the casting process step by step for the previously shown PneuNet design. Prerequisites are that the mold is 3D printed, the M4 nut is glued in place, a piece of fabric is cut to size and the operator takes necessary safety precautions.

1. Apply release agent to both parts of the mold and the M4 screw.
2. Mix the silicone and silicone thinner.
3. De-gas the silicone mixture in a vacuum chamber.
4. Insert the M4 screw into the bottom mold.
5. Fill the bottom mold with silicone mixture up to the rim.
6. Place the top mold onto the bottom mold.

7. Tighten the M4 screw until it makes contact with the inner wall.
8. Fill the top mold with approximately 5 mm of silicone mixture.
9. De-gas the silicone mixture again by placing the entire mold in the vacuum chamber.
10. Stop the degassing when there are 2 minutes left of the pot life.
11. While degassing, impregnate the fabric by applying an even layer of silicone over the entire piece of fabric.
12. De-mold the soft actuator after the cure time has elapsed.
13. Glue the soft actuator onto the fabric using silicone or silicone glue.

4.4.2 Casting Process Step by Step - McKibben

1. Apply release agent to all mold parts.
2. Put the core in the bottom mold
3. Mix the silicone and silicone thinner.
4. De-gas the silicone mixture in a vacuum chamber.
5. Fill the bottom mold (with core inserted) with silicone mixture up to the rim.
6. Place the top mold onto the bottom mold.
7. Fill the top mold with approximately 5 mm of silicone mixture.
8. De-gas the silicone mixture again by placing the entire mold in the vacuum chamber.
9. Stop the degassing when there are 2 minutes left of the pot life.
10. De-mold the silicone hose after the cure time has elapsed, but leave the core in.
11. Wind copper wire in the grooves on the rubber hose, clockwise and counter-clockwise
12. Mix the silicone and de-gas it.
13. Pour the silicone into the sealing mold.
14. Put the silicone hose (with core still inserted and wire winded around it) in the sealing mold.
15. Scrape of any excess silicone on top of the sealing mold and tape down the hose.
16. Let the silicone cure and de-mold it.
17. Apply silicone to the end caps, insert them in the ends, and fasten them with wire.
18. Glue the soft actuator onto the fabric using silicone or silicone glue.

4.4.3 Material Choice

When comparing the two different soft actuator designs, PneuNet and McKibben, it would also be interesting to compare different materials. The choice of materials in this project are somewhat based on availability, therefore all the material used are from Smooth-On, Inc. The specific silicones used can be seen in Tab. 4.2. However, Ecoflex™ GEL 2 was soon eliminated since it was too soft and thus not being able to keep its shape. Unfortunately, Elastosil M4601 was not available at Smooth-On, Inc. and therefore not used.

Material	Shore hardness
Ecoflex™ GEL 2 [102]	000-34
Dragon Skin™ FX- Pro™ [103]	02A
Dragon Skin™ 20 [104]	20A
Dragon Skin™ 30 [105]	30A
Smooth-Sil™ 945 [106]	45A

Table 4.2: Table of all the materials used and their respective shore hardness.

5

Prototype Device

To gather the readings from the sensors, control the soft actuators and communicate with the user, a prototype device will be assembled. The device will consist of a platform that houses the electronics. All devices will be controlled by software taking input from a user.

5.1 Platform

The platform was, similar to most of the hardware, designed using the CAD software Catia V5. It was designed to keep four linear actuators, four syringes, and all the necessary electronics to control the system. To make it as compact as possible the platform was split into three floors. When designing the platform, two crucial aspects had to be considered. Firstly, the linear actuators and syringes needed to be precisely aligned to achieve optimal performance. Secondly, the wire connections and electronics had to be easily accessible for maintenance and troubleshooting. This was accomplished by elevating the linear actuators to align with the syringes and also keeping the electronics on top of the platform. The complete platform with all its parts can be seen in Fig. 5.1.

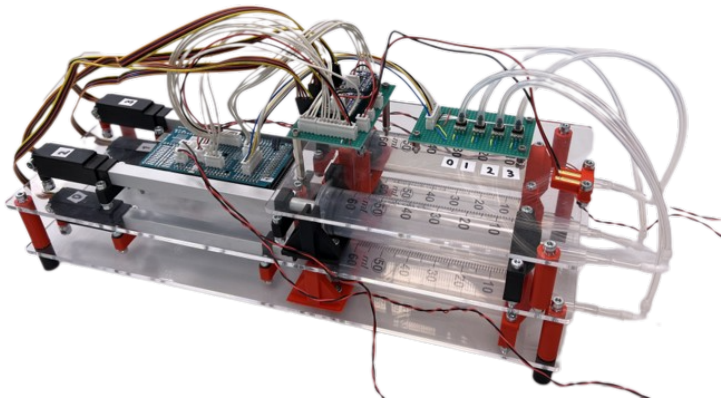

Figure 5.1: Platform.

5.1.1 Control Software

The Arduino Mega microcontroller runs a control loop that can both extend and retract each linear actuator and regulate their position with its own PID controller. The PID controller was chosen since it is easy to implement. PID control is also model-free. Therefore, a nonlinear model of the linear actuator does not need to be developed. The gains of the PID controllers were the same for all actuators and were determined empirically with the goal of the linear actuators reaching a desired position from a control signal that is not time-varying. After further testing and iteration the controller became stable with minimal oscillations, the gains were set to $K_p = 20$, $K_i = 2$ and $K_d = 0$, with the error unit in millimeters. K_d was set to zero since it causes instability in the controller.

The microcontroller is connected via its USB-B port to a PC to which it sends and received data using serial communication. In the microcontroller's control loop, live readings from each pressure, force and flex sensor are sent to the PC along with the time since the microcontroller was started, and the speed, PWM signal and position of each linear actuator. At the same time, the microcontroller also reads incoming commands from the PC. These commands include what positions to set the linear actuators to, or if to extend or retract the actuators at a certain speed.

5.2 Human-Machine System Integration

Stroke rehabilitation plays a crucial role in helping individuals regain motor function and improve their quality of life after experiencing a stroke. In order for the patient to use the rehabilitation glove independently, it is important to develop intuitive and user-friendly technologies for stroke patients, considering that a significant proportion of stroke cases occur in older adults. Approximately 75% of those affected by stroke are above 65 years old [13].

The initial stage of developing an intuitive control system for the rehabilitation glove involves selecting an appropriate input signal. One approach that enhances intuitiveness is to interpret the movements of the non-impaired hand and replicate them on the stroke-affected hand. This can be accomplished by wearing an sEMG armband on the non-impaired hand, which captures the corresponding muscle signals and translates them into control commands for the soft actuators within the rehabilitation glove worn on the stroke-affected hand. Compared to conventional methods like button pressing, this control method offers a more natural and intuitive means of operating the glove. By leveraging the patient's own movements, this approach aligns with their intentions and facilitates a seamless interaction with the rehabilitation glove. However, this project will only provide a simple control algorithm that either performs a closing or opening gesture with the hand.

To enable more precise and specific control, controlling each soft actuator independently and performing various exercises, a Graphical User Interface (GUI) has to be developed. This will, along with the sEMG, be presented and described further in this section.

5.2.1 sEMG

First of all, the armband chosen to be used in this project was the Myo Armband by Thalmic Labs. The sEMG data will be measured from the armband when two gestures are performed by the user, 'Open' or 'Close'. Open is when all the fingers are extended and close is when all the fingers are tightly curled inward towards the palm, a gripping position. This was achieved by using the classifier provided by the PyoMyo library [69]. The classifier was trained by recording the sEMG data when the user had their hand 'Open' and 'Close' respectively. The data was saved in two separate files, then the model was trained on that data and could thereby predict the correct gesture in real-time. The predicted gesture is saved in a variable that can then be sent to the linear actuator control.

5.2.2 Graphical User Interface

In order for a user to operate the system, a graphical user interface (GUI) is a much needed simplification compared to using a command line interaction. In Fig. 5.2, you can see the prototype software developed in Python. Here, the user can choose to control either the position or velocity of each individual finger. Via the sEMG button, the user can also choose to use the Myo armband in order to toggle between an extended or retracted state of the actuators.

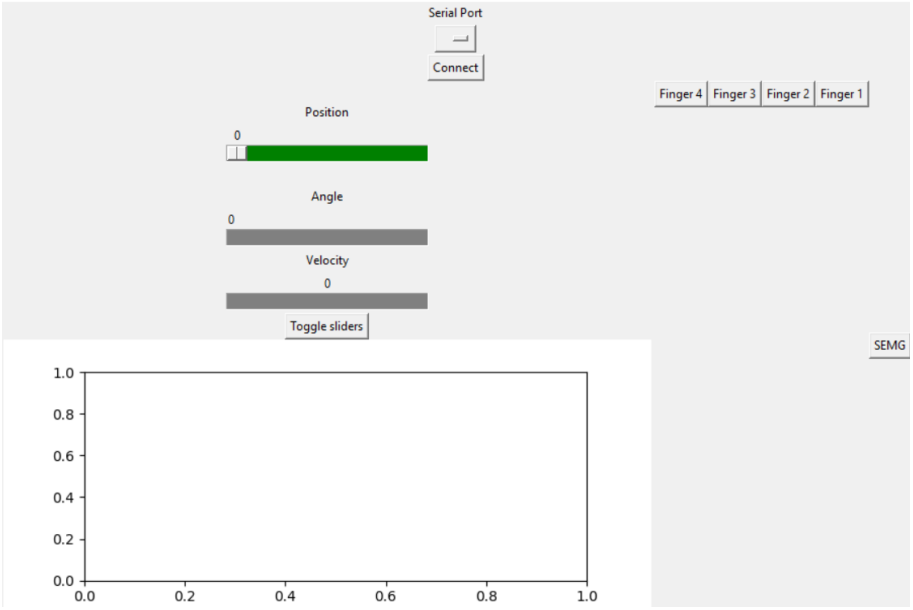

Figure 5.2: GUI.

5.3 Glove Design

This section presents two different glove designs, one for the PneuNet soft actuator and one for the McKibben soft actuator. Both finger sleeve designs enable mounting of the soft actuator onto a glove and thus construction of the rehabilitation glove.

5.3.1 Glove Design for PneuNet

An important aspect of the glove design is making it adjustable, allowing it to be worn by individuals with varying hand sizes. This was done by using velcro to mount the different fingers onto the main glove. Another important aspect was minimizing any obstruction hindering the fingers to bend. One way of minimizing this was by not casting in the flex sensor in the glove, instead only mounting it at the fingertip letting it slide freely along the finger. The finger itself consists of two main components, the soft actuator, and the finger sleeve. The finger sleeve consists of one pocket for the user's fingertip to slide into (bottom of Fig. 5.3). Furthermore, two layers of fabric were sown together with a longitudinal offset and a middle channel for the flex sensor (Fig. 5.3). The offset enabled mounting of the flex sensor only at the top but still keeping it protected inside the finger, while the channel enables it to slide freely. The complete finger sleeve can be seen in Fig. 5.6.

To then assemble the soft actuator and the finger sleeve, a multiple-step process was required. The first step was done by inserting a stick into the flex sensor's pocket. The soft actuator was then glued onto the top fabric of the finger sleeve (Fig. 5.3). The second step was to replace the stick with the flex sensor and mount it at the fingertip, with for example tape. The front part was then glued together. To attach the completed finger onto the glove itself, velcro was glued onto both, as said earlier. The glove itself had to be adjustable and well fastened onto the hand. This was done by attaching a velcro at the wrist, acting as a tightening buckle. The final glove can be seen in Fig. 7.11.

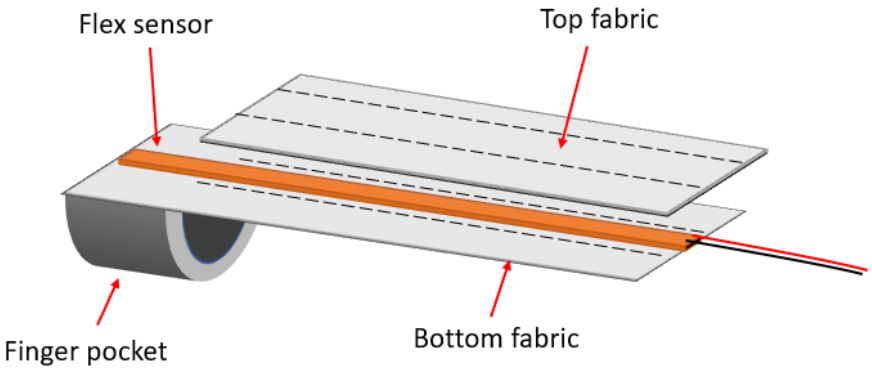

Figure 5.3: Exploded view of the finger sleeve for the PneuNet actuator.

Figure 5.4: Complete PneuNet finger displayed on a human hand.

5.3.2 Glove Design for McKibben

The design of the main glove is the same for both the PneuNet and McKibben acuator. However, the design of the finger sleeves differ to some extent between the two. Instead of gluing the actuator on the sleeve, two pockets were integrated that holds the the McKibben actuator in place. Being able to avoid the gluing process makes the manufacturing quicker and less complicated. The principal layout of the finger sleeve for the McKibben actuator can be seen in Fig. 5.5.

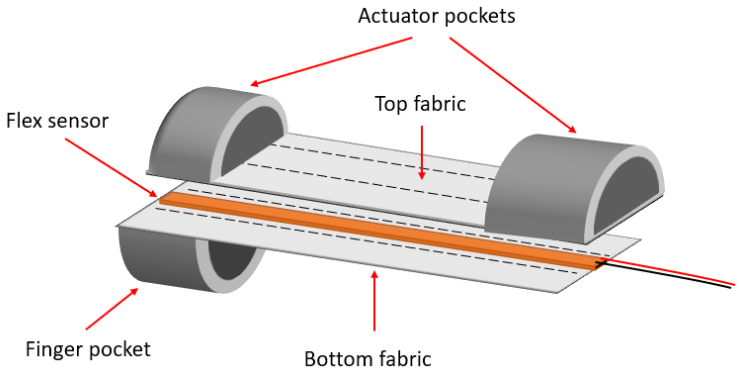

Figure 5.5: Exploded view of the finger sleeve for the McKibben actuator.

Figure 5.6: Complete McKibben finger displayed on a human hand.

6

Methods for Measurements and Data Analysis

In order to develop and verify the most suitable material and design for the soft actuators in the rehabilitation glove a range of tests have been designed. These include tests that will cover the force output and range of motion of each design and material. The design of the hardware necessary in order to conduct these tests will also be discussed.

6.1 Experimental Setups

The soft pneumatic actuators will be compared based on their fingertip force and their ROM. This is necessary to ensure that the soft actuators are able to perform ADL tasks. Therefore, experimental setups that can gather the relevant data along with experimental procedures are required. Two experimental setups were developed: one that can measure the fingertip force of each actuator, and one that can measure the bending and motion of each actuator. Both are necessary for comparing the actuators and ensuring their effectiveness for ADL tasks, but the second experimental setup will also be used to develop the empirical model that can predict the bending of the soft actuators. The experiments and experimental platforms developed make use of the prototype device that houses the electronic components and software.

6.1.1 Force Measurement Platform

The force measurement platform used for this project, which can be seen in Fig. 6.1, is designed to closely match the principal sketch presented by Polygerinos et al. [9] (Fig. 3.10), although some additional functions are added. For instance, the height of the constraining top layer can be adjusted by turning four screws, therefore allowing for actuators of different heights to be tested. Furthermore, oblong tracks were added to the platform's bottom plate, which enables easy adjustment of the distance between the proximal end attachment and the load cell. Hence, actuators of different lengths could all be tested using the same rig. Additionally, fasteners for the syringe and the linear actuator were implemented. Lastly, slots to mount the load cell were added. The load cell is connected to the HX711 amplifier that is in turn connected to the microcontroller onboard the prototype device. The platform

was partly laser cut using 3 mm acrylic sheets and partly 3D printed.

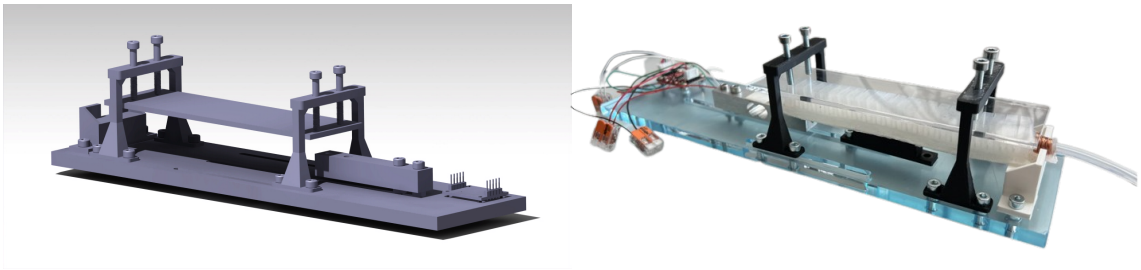

(a) CAD model **(b)** Real platform

Figure 6.1: CAD model of force measurement platform (left) and the actual force measurement platform (right).

6.1.2 Motion Measurement Platform

To evaluate the motion and bending of the soft actuators, fiducial markers were used and a motion measurement platform was built. The fiducial markers chosen were ArUco markers since there is a ready-made library for ArUco marker detection [74] and each marker has a unique ID. The markers were placed on white 3D printed cubes. These cubes were stitched to the glove on top of every joint, as well as the fingertip. The unique ID of every marker can be used to determine which joint has been detected.

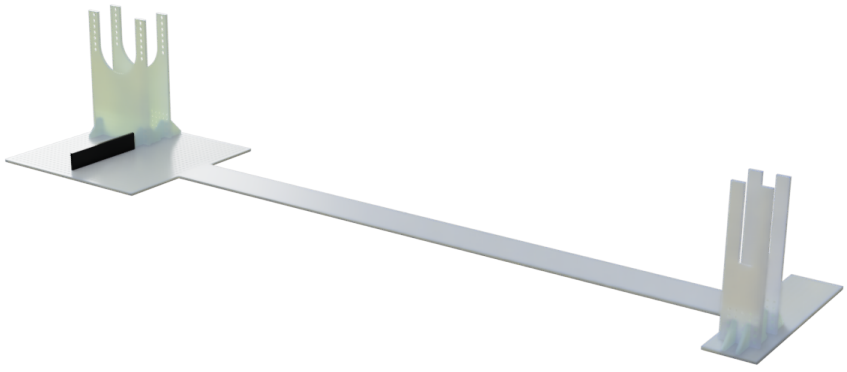

Figure 6.2: Rendering of the motion measurement platform CAD model.

The platform consisted of a long base with connections for a camera stand on one end and connections for a wrist mount and ruler on the other end (Fig. 6.2). All of the parts were made using 3 mm acrylic sheets and a laser cutter. The connections were made between 3 mm square holes. The camera stand has slots for a smartphone

with a 240 fps slow-motion camera with high-definition video capture. Slow-motion video capture is used to lessen motion blur which makes ArUco marker detection more difficult. The wrist mount is added so that the hand wearing the glove, and therefore the soft actuators, are in roughly the same spot in every video. The ruler has small markings that are 1 mm apart and larger markings that are 5 mm apart. These markings are used as a reference to convert the pixels in the video recording to millimeters in the data analysis. The ruler is placed directly underneath the ArUco markers and is approximately 78 cm away from the camera along the length of the platform. Furthermore, a red LED is used and placed in the camera frame in order to sync the video with the measured data.

6.1.3 Experimental Procedures

Below, the experimental procedures to measure fingertip force, motion, and noise level are described.

Force Measurement Procedure

To perform a fingertip force test, the distances have to be adjusted to the soft actuator. The soft actuator is then placed on the back stand (Fig. 6.1 a) and the force measuring component (seen to the right in Fig. 6.1 b). The constrained top layer is then lowered until the load cell measures a value greater than 0, preferably a value close to 0. The internal pressure of the soft actuator is then increased while the pressure and output force are being measured. When the maximum inner pressure before failure for the soft actuator is reached the test ends and the data is saved.

Motion Measurement Procedure

To perform the motion measurement, a camera is placed in the camera mount. The operator wears the glove equipped with the ArUco markers on the index finger and places their wrist in the wrist stand. To perform the test, firstly, the camera is turned on and starts recording using 3X zoom. Then, when a connection between the PC and the microcontroller is established, the LED light flashes once, signaling that the sensors are being read and sampled. The linear actuator then actuates the soft actuator, making the operator's finger bend. When the soft actuator reaches its maximum inner pressure, the test ends and the data is saved. Afterwards, the video recording and sensor data is analyzed and the time to fully actuate is noted.

Noise Level Measurement Procedure

The noise levels during the actuation of the soft actuators were measured at a distance of 1 meter using the app "Buller" [107] on a smartphone (iPhone 13 Pro). Measurements of the mean and maximum noise level were taken for the full stroke length of the syringe pumps, 1, 2, 3 and 4 syringe pumps at a time. The ends of each linear actuator was sealed, simulating the force from any soft actuator.

6.2 Data Analysis

In this section, the processing of the collected video data during motion measurement testing is described. Furthermore, the synchronization of the video and sensor data for the optimal soft actuator is described. The combined dataset of video and sensor data is used to create linear regression models that can predict the bending angle of the optimal soft actuator.

6.2.1 Computer Vision Algorithm

To capture the motion and bending angle of the actuator, a computer vision algorithm was developed. The algorithm consists of four main parts: (1) video recording; (2) marker detection; (3) coordinate rotation; and (4) angle calculations. (1) A video file from an experiment is read and saved as a list of images, or frames. Every frame is then analyzed. (2) Firstly, the frame is analyzed for markers by a detection algorithm. Here, OpenCV's ArUco detection module is used [74] since the library is widely available and fast to implement. (3) After the markers have been detected, the MCP and CMC joints are used to rotate the marker positions. The vectors of the joint positions are transformed via translation so that the MCP joint is positioned in the origin (0,0). Then, all joint vectors are rotated so that the vector from the MCP to the CMC joint is horizontal, i.e. parallel with the x-axis. If the MCP or CMC joint is not detected, then the rotation cannot be made and this frame is not analyzed further. The coordinates of the markers are also scaled from pixels to millimeters using a scaling factor developed using the ruler from the motion experiment as a reference. (4) Finally, the angle between the different markers are calculated using rudimentary linear algebra. This includes the angles of the vertices of the MCP, PIP and DIP joints, i.e. the bending angle of each finger joint, and the bending angle θ_{bending} (Fig. 6.4). An overview of the complete computer vision algorithm can be seen in Fig. 6.3.

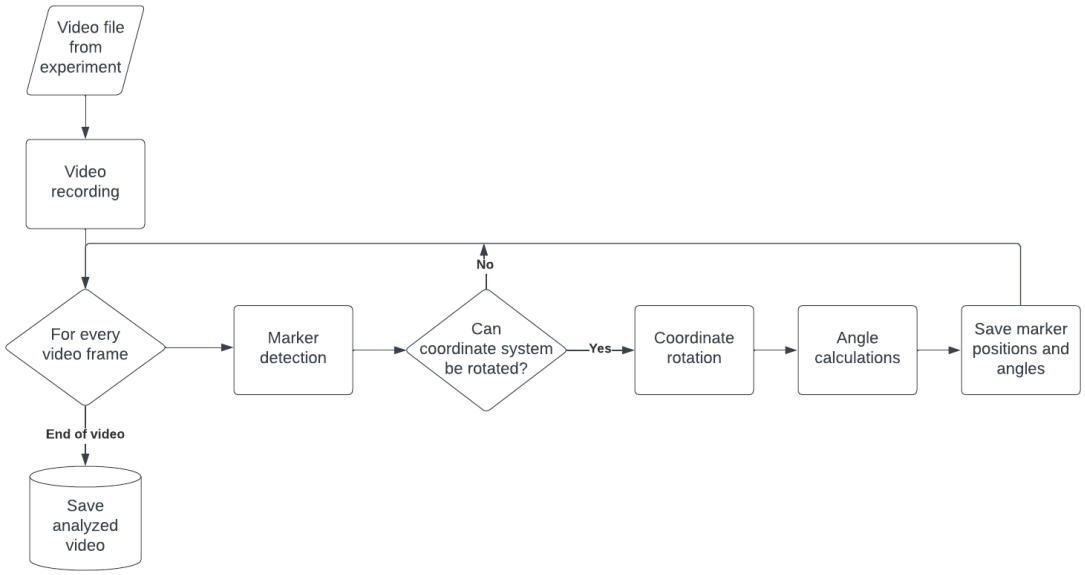

Figure 6.3: Flow chart of the different parts of the computer vision algorithm. Among these are: (1) Video recording; (2) Marker detection; (3) Coordinate rotation; and (4) Angle calculations.

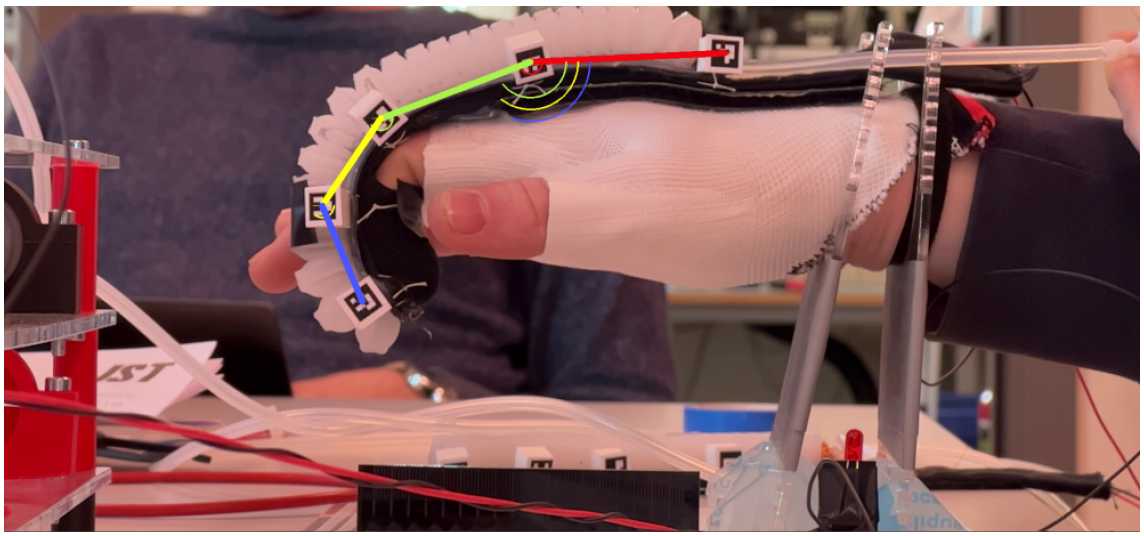

Figure 6.4: A video frame that has been analyzed. The arcs directly underneath the MCP, PIP and DIP joints show their respective joint's bending angle. The large blue arc underneath the MCP joint shows the bending angle θ_{bending}.

6.2.2 Development of the Linear Regression Models

The most suitable soft actuator is determined by the force, motion and noise level measurements. To develop a bending angle filter, the data from the sensors are combined with the bending angle data. The bending angle θ_{bending} at each time step is calculated in the computer vision algorithm. The timestamp when the sensor

readings start can be found in the video frame when the LED blinks, which is used to synchronize the data. Since the bending angles are captured at a higher frame rate than the sensor data, the bending angles are interpolated to fit the time steps of the sensor data. The datasets used come from three separate experimental trials of the most optimal soft actuator. The observations from two of the trials are used for the training dataset while the third trial is used for the testing dataset which will be used to validate the three models. For each model, the R^2 and standard error are calculated. After the models have been created, the MSE and standard deviation are calculated using the testing dataset.

7

Results

This chapter presents the results obtained from the testing performed on different soft actuator designs and materials. The testing aimed to evaluate the performance of the soft actuators in terms of force, bending angle and speed, as well as noise level measurements and linear regression models. The results are presented using tables, graphs and figures to provide a comprehensive understanding of the findings. Because of the softness of the silicon with shore 02A, the PneuNet actuator with that silicon did break during the testing process before a result could be obtained and are therefore not presented. In the end, the final prototype is shown.

7.1 Force Testing

The results from the testing of maximum fingertip force for different silicones and actuator designs are displayed in Tab. 7.1. The forces for each measurement were also plotted as a function of the internal pressure, and can be seen in Fig. 7.1 and Fig. 7.2.

Type of Soft Actuator	**Material**	**Max. Force**	**Max. Pressure**
PneuNet	20A	18.04 N	0.99 bar
PneuNet	30A	19.39 N	1.52 bar
PneuNet	45A	8.49N	1.97 bar
McKibben	02A	3.91 N	0.72 bar
McKibben	20A	8.38 N	1.83 bar
McKibben	30A	7.92 N	1.98 bar
McKibben	45A	3.08 N	2.08 bar

Table 7.1: Table of max. force and max. pressure for each of the soft actuators tested.

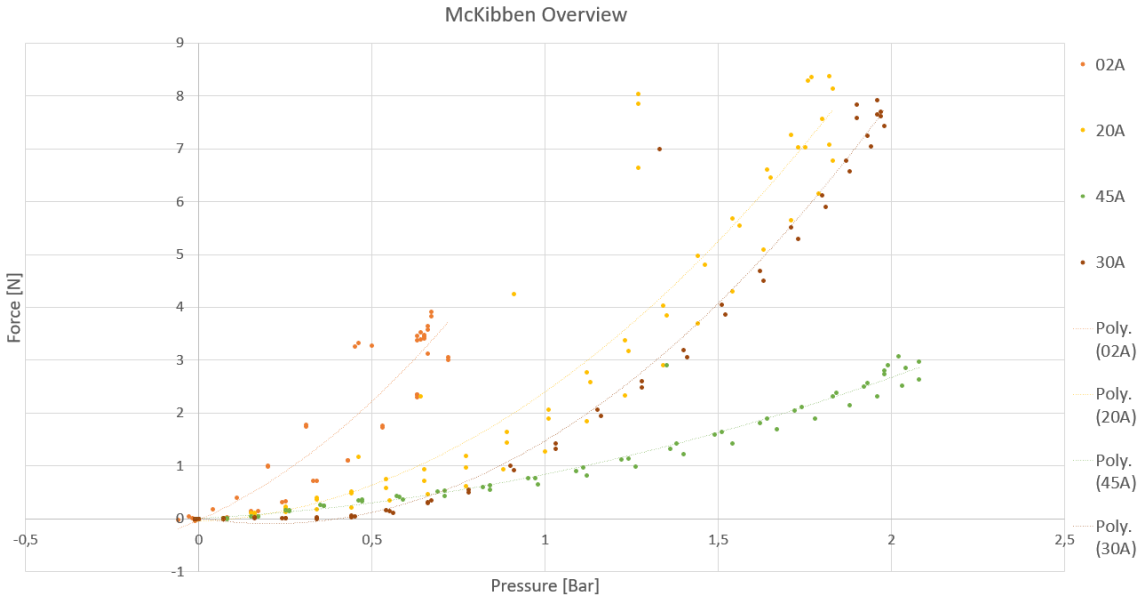

Figure 7.1: A visualisation that shows the force applied to the load cell versus internal pressure of the McKibben actuators.

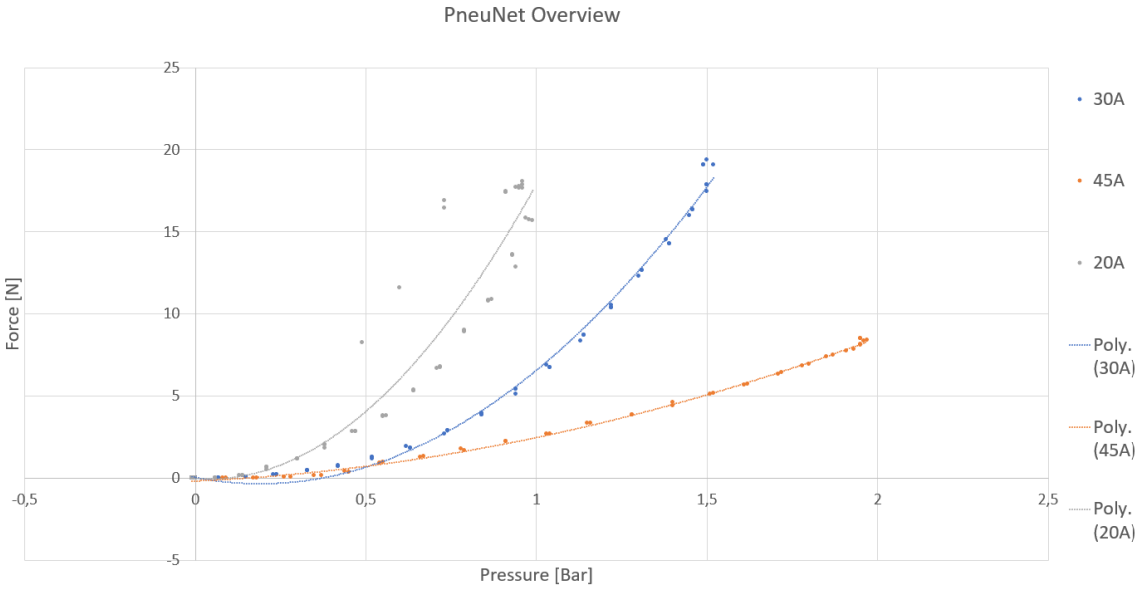

Figure 7.2: A visualisation that shows the force applied to the load cell versus internal pressure of the PneuNet actuators.

7.2 Joint Range of Motion and Actuation Speed

In this test and in following results PneuNet 45A will not be considered as when the test was conducted the bending of the actuator was insufficient to show a meaningful result. In Fig. 7.3, Fig. 7.4 and Fig. 7.5, the bending angle of each joint is displayed. The y-axis shows how much the actuator bent the joint from its minimum position.

The x-axis shows what actuator type and what stiffness was used. In addition the averages and standard deviations are shown in Tab. 7.2.

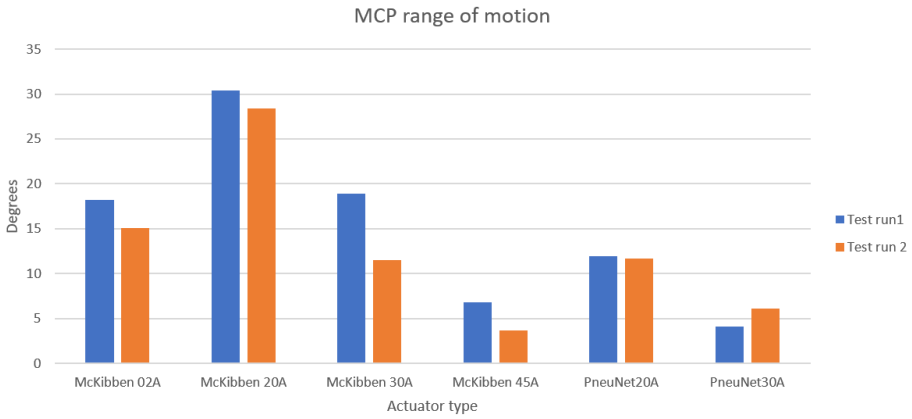

Figure 7.3: ROM of the MCP joint.

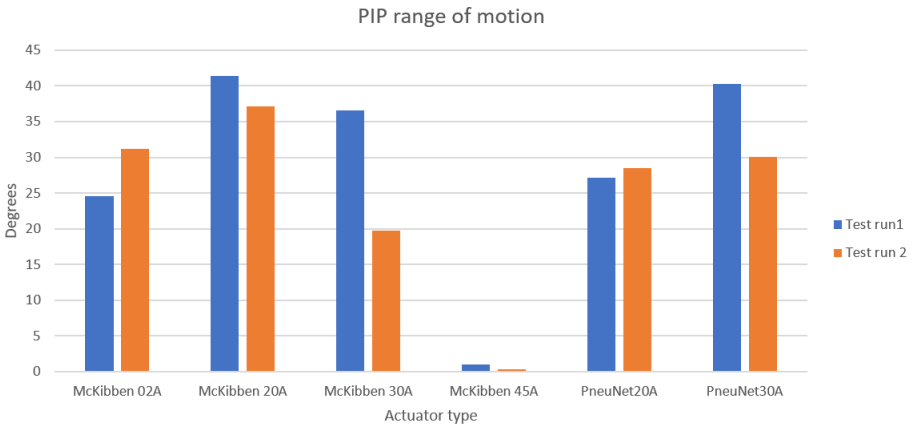

Figure 7.4: ROM of the PIP joint.

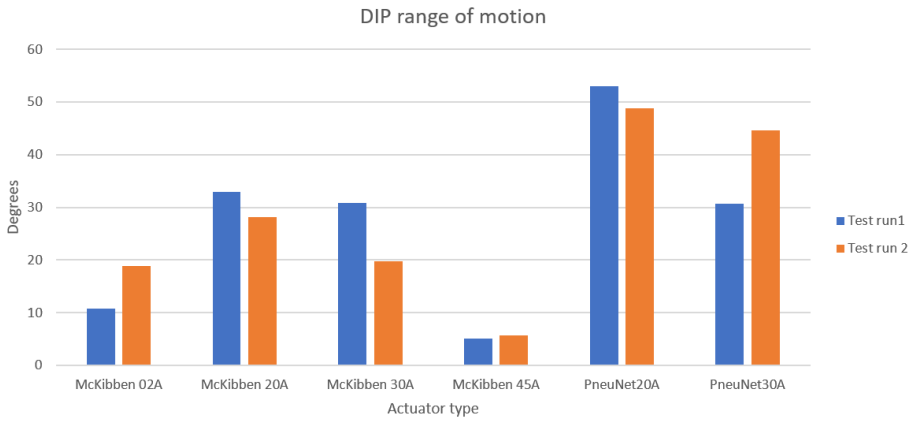

Figure 7.5: ROM of the DIP joint.

Actuator	MCP mean [°]	PIP mean [°]	DIP mean [°]
McKibben 02A	16.6 (SD 1.5)	27.9 (SD 3.3)	14.8 (SD 4.1)
McKibben 20A	29.4 (SD 1.0)	39.3 (SD 2.1)	30.5 (SD 2.4)
McKibben 30A	15.2 (SD 3.7)	28.1 (SD 8.4)	25.2 (SD 5.5)
McKibben 45A	5.2 (SD 1.5)	0.6 (SD 0.3)	5.4 (SD 0.3)
PneuNet 20A	11.8 (SD 0.1)	27.8 (SD 0.7)	50.9 (SD 2.1)
PneuNet 30A	5.1 (SD 1.0)	35.2 (SD 5.1)	37.7 (SD 6.9)

Table 7.2: Average joint bending angles and range (maximum ROM result - minimum ROM result) of range of motion tests.

The time it took for full actuation was around 4 seconds, which is shorter than the requirement of 5 seconds. The bending angle at a given time for one of the project's soft actuator is displayed in Fig. 7.6. By measuring the time difference between the lowest yellow elbow in the bottom left to the top left yellow elbow, a time of around 4 seconds is obtained. The actuation system is consequently assessed fast enough for the application. All joint angle plots can be found in Appendix. A.1.

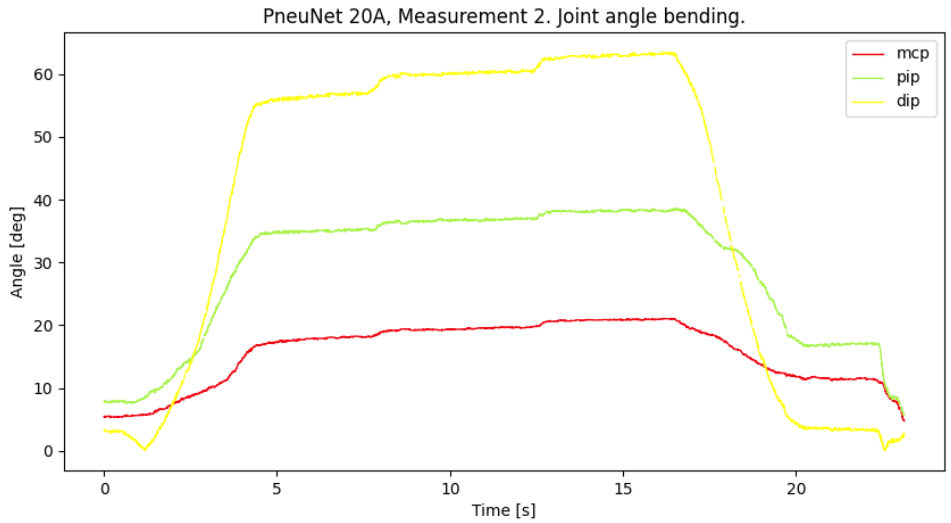

Figure 7.6: Joint angle bending vs time, PneuNet 20A.

7.3 Motion traces

In Fig. 7.7, Fig. 7.8 and Fig. 7.9, the motion traces of a McKibben 20A, PneuNet 20A and a hand without any soft actuator respectively are shown. Additionally, all motion traces can be found in Appendix. A.1.

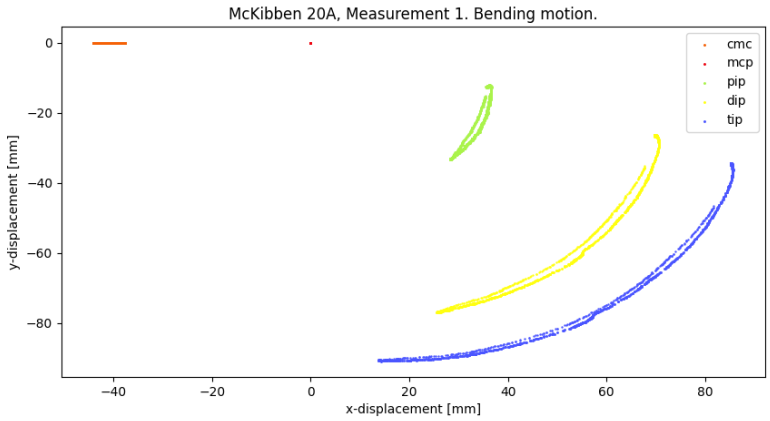

Figure 7.7: Motion trace of the McKibben 20A.

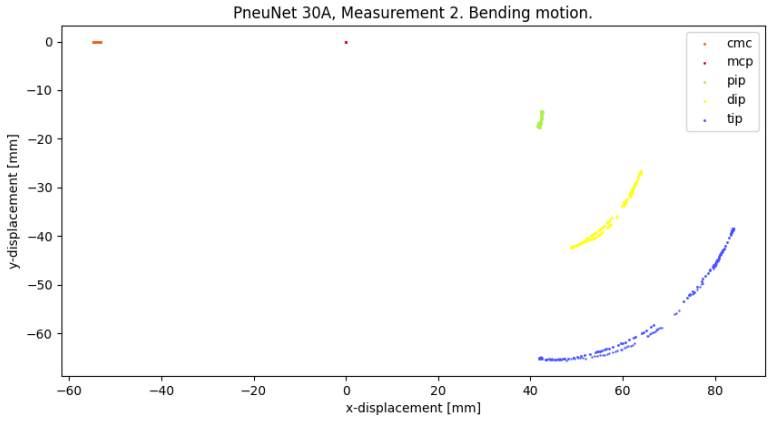

Figure 7.8: Motion trace of the PneuNet 20A.

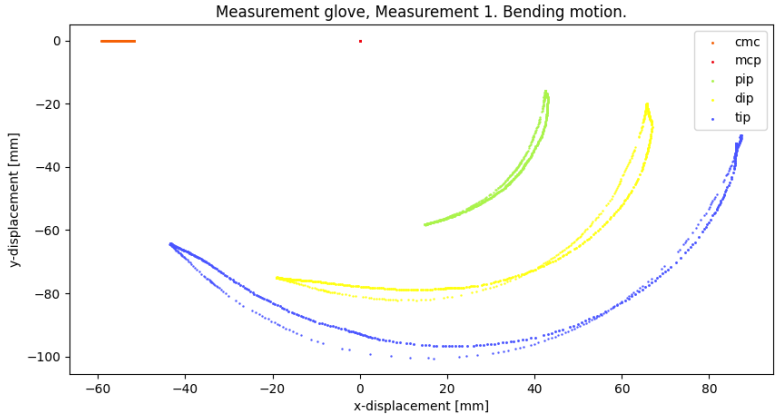

Figure 7.9: Motion trace of a hand without a soft actuator attached.

7.4 Noise Level

The results from the noise level measurements can be seen in Tab. 7.3. The measurements show that the device does not exceed the noise level of normal conversation, and consequently does fulfill the noise requirements previously stated in Sec. 4.1.

Number of actuators	Avg. noise level [dBA]	Max. noise level [dBA]
1	48.3	54.1
2	53.3	59.2
3	55.2	60.0
4	57.0	60.0

Table 7.3: Average and maximum noise levels during actuation.

7.5 Decision of the Optimal Soft Actuator

The most suitable soft actuator type for this project turned out to be the pneumatic soft actuator. The PneuNet and McKibben designs were tested and compared in order to determine the optimal design.

The force measurements show that the PneuNet design clearly can exert the highest fingertip force among the two actuator types. More specific, the PneuNet with silicone stiffness 30A was found to be the strongest (19.39 N), slightly exceeding the PneuNet with silicone stiffness 20A (18.04 N). Therefore, these two actuator type-material combinations satisfy the specified force requirement of 10.5 N.

The PneuNet also turned out to perform best with regards to bending performance, PneuNet 20A and 30A outputting a cumulative bending angle of all joints of 90.5° , and 78.0° respectively. Since both silicone stiffnesses allow adequate fingertip force for ADL, the bending performance was assessed to be the decisive performance category. On that basis, the PneuNet 20A was considered the most suitable one to be fit on a rehabilitation glove. However, no actuator met the requirement of achieving full range of motion in each joint.

7.6 Linear Regression Models

After determining that the PneuNet 20A is the most optimal soft actuator design, three motion experiments were used to develop the three linear regression models. The sensor data was sampled with a mean frequency of around 3.1 Hz. There were 206 observations in total, of which 46 were used for the test dataset. The linear regression models were validated using the test data (Fig. 7.10) and their R^2, standard error, MSE and SD were calculated (Tab. 7.4).

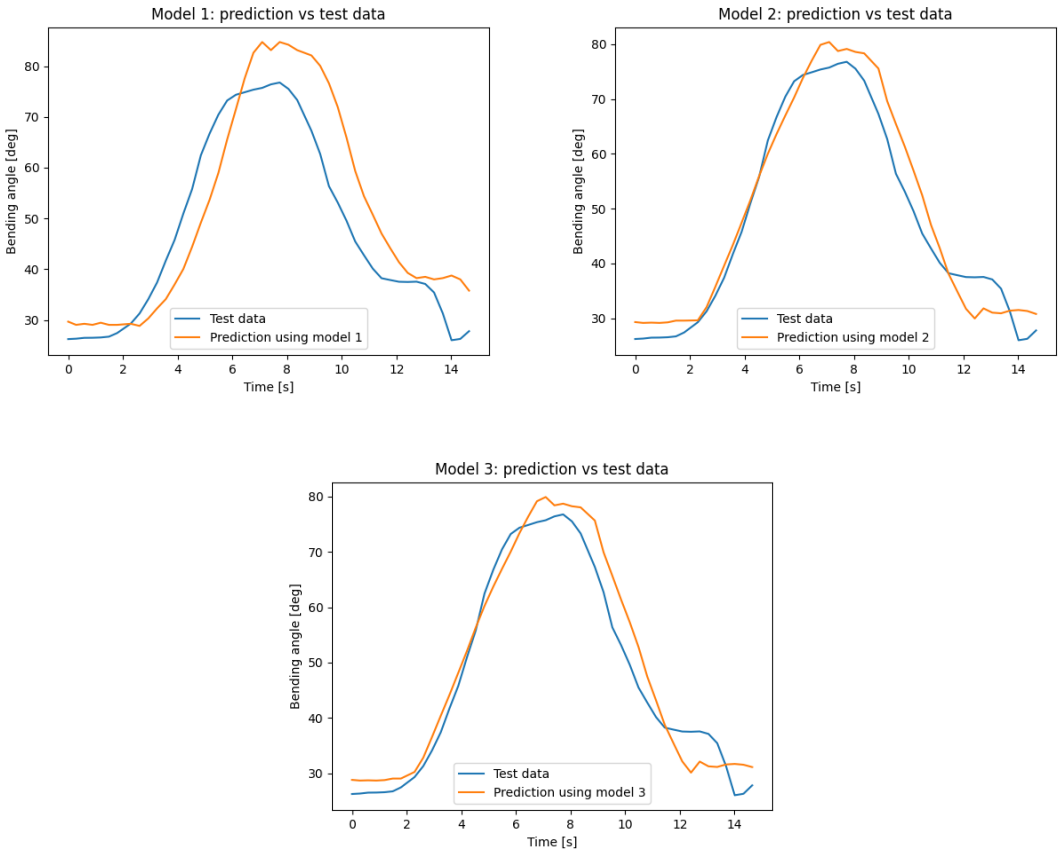

Figure 7.10: Linear regression models using PneuNet 20A experimental data. Model 1: trained on flex resistance. Model 2: trained on flex resistance and internal pressure. Model 3: trained on flex resistance, internal pressure and linear actuator position.

Model	R^2	Standard error [deg]	MSE [deg^2]	SD [deg]
Model 1	0.925	5.562	86.90	18.13
Model 2	0.976	3.158	18.31	18.13
Model 3	0.976	3.130	18.24	18.13

Table 7.4: Comparison of the regression and error statistics for three models.

7.7 Final Prototype

The final glove can be seen in Fig. 7.11The weight of the glove including the soft actuators is 180.1 g, weighted with a table scale (Kern PCB 6000-1). Thus the glove well meets the requirement of 0.5 kg. An emergency stop was also implemented successfully.

Furthermore, the goal of the glove being able to perform grasping and have individual control of each finger was achieved with restricted ROM. This is displayed in Fig.

7.12, where the grasping exercise is performed. Additionally, in Fig. 7.13, the individual control of each finger is shown.

The goal of creating an intuitive and user-friendly control was done by implementing an user-friendly GUI as seen in Fig, 5.2. Software for the sEMG armband to control all the fingers simultaneously was also developed, however not successfully implemented.

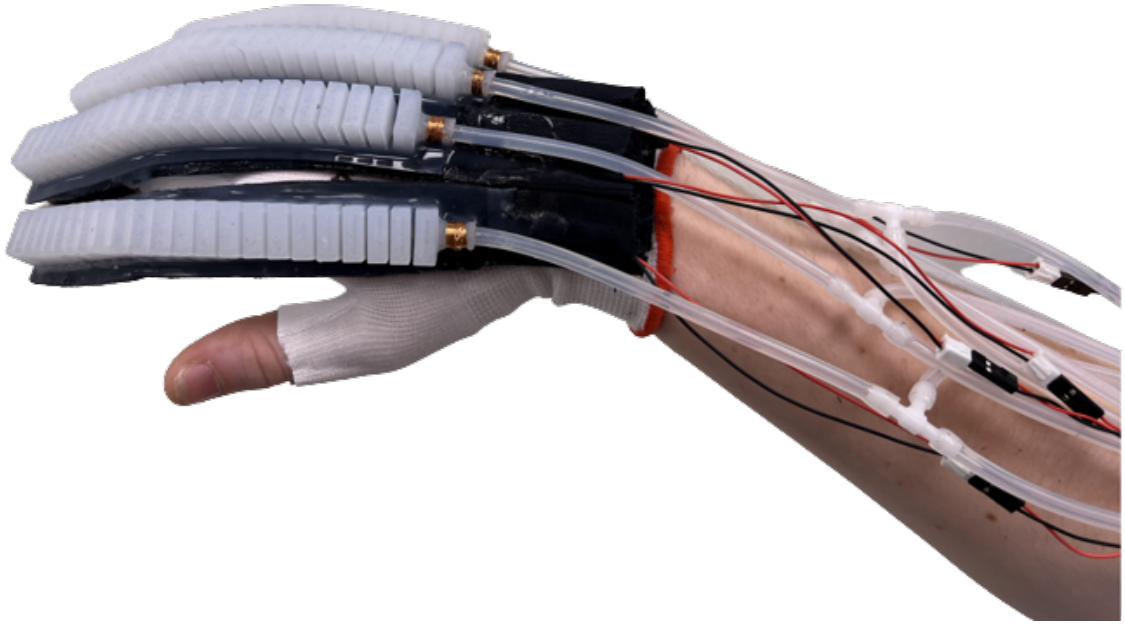

Figure 7.11: Completed final glove.

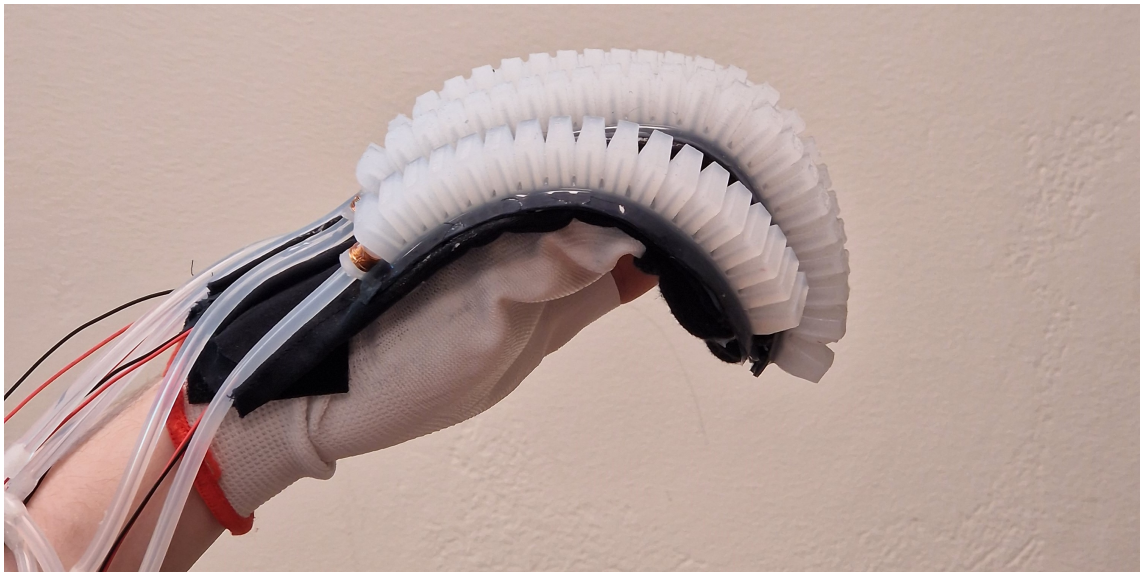

Figure 7.12: Full grasping of prototype.

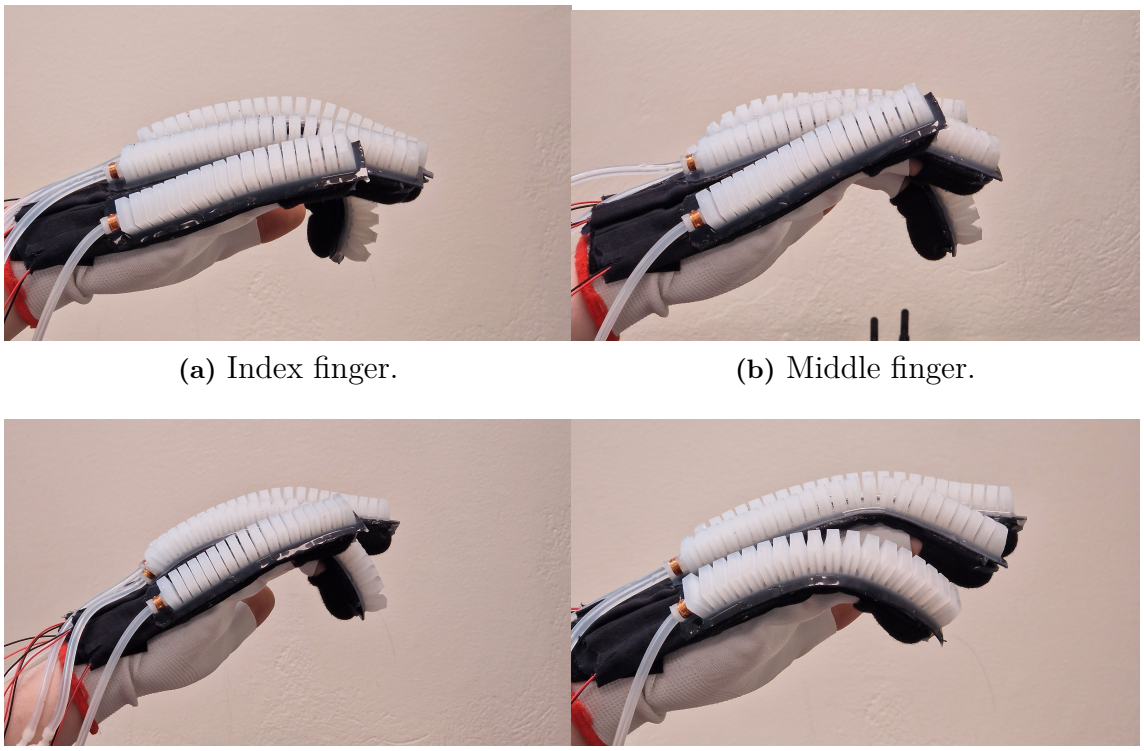

(a) Index finger. **(b)** Middle finger.

(c) Ring finger. **(d)** Little finger.

Figure 7.13: Finger movement for individual finger.

8

Discussion

The results presented will be further discussed to highlight the strengths and limitations of the project, and bring up potential sources of error that could have affected the result. It will also be compared with existing literature to give a perception of what has been done and what can be developed further.

8.1 Interpretation of Results

In the following section, the results from force testing and bending angle testing will be discussed, as well as potential error sources that could affect the results. The PneuNet 02A was not tested for any experiment since it could not handle being pressurized. The material was too soft which caused excessive swelling which prevented the soft actuator from bending.

8.1.1 Force Testing

From Tab. 7.1, it is clear that the PneuNet design outperforms the McKibben design. No other soft actuator type-material combination than PneuNet 20A and PneuNet 30A satisfies the fingertip force requirement for ADL (10.5 N) [28].

Sources of Error

The adjustable constraining top layer comes with the advantage of testing multiple different actuators with the same test rig. However, using adjustable pieces in a measuring rig is a risk since it often contributes to the tests not being performed identically to each other. If the top layer was tightened too hard, it could result in a much larger force obtained from the force test. The problem was solved by tightening the top layer until the load cell starts to notice a difference in force. Another error could be that the top layer is uneven (not parallel to the bottom plate), this could also result in the soft actuator not performing optimally. This could, together with the error of tightening the top layer too much, be minimized by implementing positional readers for all the screws or redesigning the adjustment.

The amount of internal pressure that the actuators were able to withstand before failing, was assessed simply by visual inspection. The judgment of the observer may therefore heavily influence the actuation pressure that the actuators are tested with. Some actuators would maybe tolerate even higher strains before failing, and thus

generate higher forces. To avoid the impact of human factors, one could have tested at which pressure each actuator normally fails.

Another factor that needs to be taken into consideration observing the test result, is that the forces are generated during close to maximum pressure before failing. Such magnitude of actuation pressures may not favor reliability and are possibly not feasible to implement in a frequently used device. To decide which pressures can be applied (and what fingertip forces such pressures would induce) regularly without failing, fatigue life analysis could be a solution.

A systematical error that occurs when using a load cell previously mentioned is that this unit only measures force applied in one direction. This means that all components of the force applied not going parallel to the z-line will not be recorded in the tests. This is however mitigated by the previously mentioned modified test setup as the constrained top layer will minimize movement in x- and y-directions. A more suitable solution to know the resultant force outright is to use a multi-axial load cell but this would not fit in the budget constraint of the project.

8.1.2 Range of Motion Testing

In Fig. 7.3, Fig. 7.4 and Fig. 7.5 the ROM for the different joints can be seen. As mentioned in Sec. 7.2 the PneuNet 45A actuator did not produce enough ROM in order to produce a meaningful result. This could be due to a manufacturing defect although this is not of major concern as the 45A silicone did not show a desirable force characteristic and thus did not impact the outcome of the project.

As discussed in the force testing section none of the McKibben actuators satisfied the force requirements for ADL, but they do exhibit some advantageous characteristics when considering ROM. The McKibben actuators perform better in both the joint angle bending tests and mimics the unrestrained motion of a human hand more closely (Fig. 7.7 and Fig. 7.9). Although this is an advantage for the McKibben actuators, PneuNet 20A did perform sufficiently well in order for the actuator to full fill the stated requirement of performing a grasping motion. So in conclusion the advantage of the McKibben actuators in the ROM does not outweigh the insufficiency to meet the ADL force requirement.

Sources of Error

The ArUco markers placed on each individual soft actuator could be a source of error. The ArUco markers were placed on the tested actuators manually and could therefore have small differences in placement. As the same person was the test subject wearing the finger tested, the placement can be seen as accurate, with a small potential of error. The markers were also put onto 3D printed white cubes that were slightly displaced and bent during actuation, which would affect where the detected joint positions were. To prevent this, round reflective markers could have been used together with a sophisticated motion capture system. The camera also has some lens distortion which will affect the detection of joint positions. However, since the camera used 3X zoom, the effects of the distortion should be quite minimal.

In a few frames of the recorded videos, the ArUco markers could not be detected. The reason for this could be that ArUco marker detection is sensitive to motion blur. To negate this, the videos were captured at 240 fps, but it is still possible that motion blur affected the detection rate. To counteract this, CCTags or some other fiducial markers that work well with motion blur could have been used, or a camera with higher frame rate capture could have been used. Another reason why detection failed could be that the ArUco markers were simply printed on paper. The markers could be scratched which makes detection harder.

As the whole test was done on a human operating the finger, one source of error is the possibility of not relaxing the hand and restraining the bending of the actuator when pressurizing it.

8.1.3 Bending Angle Filter

The linear regression models yielded quite accurate R^2 and standard error values. During validation, however, the error in the models are prevalent. The models seem to overshoot and predict the bending angle to be way greater than the actual value suggests. The improvement from model 1 to model 2 when the pressure was included can be seen in the plots (Fig. 7.10) and in the regression and error statistics (Tab. 7.4). The improvement from model 2 to model 3 is minimal, but can be seen in both the standard error and validation MSE.

Sources of Error

There are a number of sources of error that affected the results. Firstly, the number of observations was quite small because of the low sampling rate of only 3.1 Hz. The reason for the low sampling rate lies in the code and communication between the microcontroller and the PC. The microcontroller is set up to send new sensor readings via serial before reading from the sensors again. To increase the sampling rate, the sensor data should have been saved on the microcontroller and sent to the PC after the experiment is over.

8.2 Comparison with Related Literature

In this section, comparisons to related literature will be made to evaluate the results presented in this report. The differences will be discussed and explanations as to why the differences exist will be presented.

8.2.1 Force Test

The force test used in this project was heavily inspired by Polygerinos et al. [9] and the results gathered will now be compared with their results. The soft actuator used in their project is a McKibben similar to the one developed in this project. Their McKibben was made out of the silicone Elastosil M4601, and at a pressure of 3.45 bar, they reached a fingertip force of around 8 N. The McKibben soft actuator design developed in this project achieved a force of around 8 N as well, however, at almost

half the pressure, around 2 bar. The shore hardness of Elastosil M4601 is around 28A and the McKibbens mentioned before were of shore hardness 20A and 30A. Therefore, the material difference can be overlooked. Unfortunately, Polygerinos et al. [9] are not specific in what materials they use as strain limiting layers, neither do they describe the dimensions of their design further than the cross-sectional dimensions. The specific dimensions provided are a width of 20 mm and a height of 10 mm. Compared to this project's McKibben design, where the width is 15 mm and the height is 10.6 mm. The height can be overlooked since it is a difference of only 0.6 mm. However, the width has a significant difference of 5 mm. Other than the width there could be other parameters that differ, such as the wall-thickness and the pitch of the radial strain limiting layer, which makes this project's McKibben soft actuator obtain the same force at a lower pressure.

Observing the fingertip force generated by the PneuNet actuators, they far exceed measurements done in several other works, including maximum forces of 1.6 N at 150 kPa [89], 1.28 N at 80 kPa [108], and 1.21 N at 43 kPa [32]. However, the results may vary to some degree because of different force sensors, measurement rigs, and measurement procedures. It is difficult to draw a definite conclusion whether one actuator is better than the other unless the testing conditions are identical. Nonetheless, the test conditions in terms of the measurement rig are similar to the one used by Polygerinos et al. [9]. Compared with their results (although for a McKibben type actuator), the PneuNet actuators developed in this project can output higher force. In summary, the force measurement results indicate that the actuators inherit competitive fingertip force capabilities, though to draw any definite conclusion the test conditions would have to be matched.

8.2.2 Range of Motion

The bending angles achieved by the rehabilitation glove were presented in Tab. 7.2 and compared to the work of Yap et al. [55]. The finger joint bending angles using their soft robotic glove, were 68.1° for MCP, 45.4° for PIP, and 50.8° for DIP. When put against the glove developed in this project with bending angles 11.8° for MCP, 27.8° for PIP, and 50.9° for DIP, one can see that the angles for the DIP joint closely match each other. However, the bending angles for the MCP and the PIP joint are superior for the glove presented by Yap et al. [55].

The reason that the bending angles are smaller compared to related literature, may be due to the attachment of the actuators to the fingers. When bending a finger, the actuator must elongate or glide against the back of the hand, which to some degree is restricted by the glove.

8.2.3 Bending Angle Filter

Models 1 and 2 can be compared to models 1 and 2 developed by Elgeneidy et al. [59]. Our models had higher R^2 values, slightly higher standard errors and much higher MSE and SD values. The reasons behind this could be the sources of error in the results. The validation data that Elgeneidy et al. used had the bending angle go from 0° to -15° while our bending angle went from 26° to 75°. This larger span

could have contributed to the larger MSE of our models.

Elgeneidy et al. also developed a nonlinear bending angle filter using an FNN model which has the advantage of capturing the nonlinearity of the dynamics better than linear regression. This is something that could improve our current models but would require a lot more data to be effectively trained.

8.3 Further Development

The work that has been made in this project has some limitations, some of which could be improved with further work.

The final choice of the actuator has a fingertip force of 18.04 N, which is well over the limit for performing ADL, according to Smaby et al. [28]. The FROM, on the other hand, was not fully reached. This means that the glove will be limited within the FROM we can obtain. The FROM of the actuator could possibly be improved with further development of the actuator, but it was not further investigated in this project. Investigating the parameters of the design of the actuator to explore the possibilities of full FROM could be an interesting subject for future research. Improving the glove design, specifically the finger sleeve, could also result in reaching FROM. Possible improvements could be to enable the soft actuator to slide forward even more on the back of the hand, thus bending the MCP joint further.

Another interesting aspect connected to the development of the soft actuator was the choice of glue in the manufacturing process. When manufacturing the PneuNet soft actuator, the top part had to be glued onto the strain-constraining layer for it to bend. However, the choice of glue had a big impact on the performance of the soft actuator. Using a silicone glue, Sil-Poxy™ [109], with high viscosity did not make a sealed connection between the two since it was too uneven. Instead, using silicone as glue, performed better since the spread was more even, however using silicone of different types was not successful either since they broke at a lower pressure compared to using the same type of silicone as glue. Therefore, future work should use the same type of silicone as glue when manufacturing the PneuNet soft actuator.

As stated earlier, the thumb was not included in this project, since the movement of the thumb differs from the other fingers and it would take another type of actuator to mimic its motions. Adding the thumb could be an important and big improvement for this project since it would create the opportunity to perform several different rehabilitation exercises with more complexity. The system developed in this project enables individual control of each finger, so the implementation of the thumb could be integrated with the system without any major changes. With a successful integration, exercises such as finger opposition could be possible to perform.

The developed model for the bending angle filter has some issues regarding the accuracy. As mentioned, the model can be improved by using an FNN model instead and increasing the size of the training data. Still, the results show promise and with improvements the model can be used to control the bending angle of the soft actuators. With further developments, the controller could be updated to use ILC

to account for the nonlinearities, if the tasks are repetitive enough. Alternatively, MPC could be used using the bending angle filter.

The usage of sEMG to achieve easy control of the system was briefly explored but could be further developed. Implementing the sEMG control of the system could make it much more intuitive and easy for the patient to use. In this project, binary control was developed but not implemented as there was an excessive delay between the micro controller and the software classifying the results from the myo armband. With further development this issue can be resolved, in addition real-time tracking of the movements could be done, making it possible to control multiple and complex movements using only the sEMG control, enabling intuitive control.

Furthermore, the volume of the syringes could be reduced to 44 ml to achieve a more compact system, still obtaining the current range of motion attained by the glove. This would also reduce the volume of air in the system, making the actuation quicker and more energy effective.

9

Conclusion

In this project, a prototype that could be used for common hand rehabilitation exercises was presented. The goal was to investigate the suitability of different types of actuation methods, as well as different soft actuator designs and materials for a hand rehabilitation device. Two different actuator designs were tested, the McKibben and the PneuNet, as they are the most commonly mentioned in the literature. The PneuNet design made with the silicone Dragon Skin^{TM} 20 (shore 20A) was shown to give the best overall result with respect to the force and the bending, and was selected for the prototype. Individual control for each actuator was successfully implemented, making it possible to achieve individual control of each finger. This is a prerequisite for enabling the finger opposition exercise, which by the implementation of a thumb actuator could be facilitated with the presented system. Furthermore, grasping actuation commands were enabled using sEMG sensors, although with an excessive delay between the microcontroller and the software. The bending angle filter that was developed has a high error rate and could be improved, using a nonlinear model. Nevertheless, once refined, the filter can be used to implement closed-loop control of the bending angle of the soft actuators.

In conclusion, the goals set up in the beginning of this bachelor's thesis were met, and the final prototype can be used for stroke hand rehabilitation.

References

[1] World Stroke Organization, *Global stroke fact sheet 2022*, 2022.

[2] X. Hu. "Stroke, rehabilitering." (Dec. 30, 2020), [Online]. Available: https://www.internetmedicin.se/behandlingsoversikter/neurologi/stroke-rehabilitering/ (visited on 01/26/2023).

[3] P. Tuominen. "Rehabilitering efter stroke." (2020), [Online]. Available: https://www.1177.se/behandling--hjalpmedel/smartbehandlingar-och-rehabilitering/rehabilitering-efter-stroke/ (visited on 05/04/2023).

[4] M. A. Talab, K. Péter, and H. A. Almusawi, "Design of an individual fingers rehabilitation device," in *2022 IEEE 20th International Power Electronics and Motion Control Conference (PEMC)*, IEEE, Sep. 2022. DOI: 10.1109/PEMC51159.2022.9962909.

[5] X. Q. Shi, H. L. Heung, Z. Q. Tang, Z. Li, and K. Y. Tong, "Effects of a soft robotic hand for hand rehabilitation in chronic stroke survivors," *Journal of Stroke and Cerebrovascular Diseases*, vol. 30, no. 7, Jul. 2021. DOI: https://doi.org/10.1016/j.jstrokecerebrovasdis.2021.105812.

[6] J. M. Veerbeek, E. van Wegen, R. van Peppen, *et al.*, "What is the evidence for physical therapy poststroke? a systematic review and meta-analysis," *PLoS One*, Feb. 2014. DOI: https://doi.org/10.1371/journal.pone.0087987.

[7] Flint Rehab, "Effective grasp and release activities for stroke recovery," Medicaly reviewd by Courtney Maher, OTR/L, Dec. 2019.

[8] Saebo, *25 hand exercises for stroke recovery*, Accessed on January 27, 2023. [Online]. Available: https://www.saebo.com/blog/reclaim-your-dexterity-with-hand-exercises-for-stroke-recovery/.

[9] P. Polygerinos, Z. Wang, K. C. Galloway, R. J. Wood, and C. J. Walsh, "Soft robotic glove for combined assistance and at-home rehabilitation," *Robotics and Autonomous Systems*, vol. 73, pp. 135–143, 2015, Wearable Robotics, ISSN: 0921-8890. DOI: https://doi.org/10.1016/j.robot.2014.08.014.

[10] N. S. K. Ho, K. Y. Tong, X. L. Hu, *et al.*, "An emg-driven exoskeleton hand robotic training device on chronic stroke subjects: Task training system for stroke rehabilitation," in *2011 IEEE International Conference on Rehabilitation Robotics*, 2011, pp. 1–5. DOI: 10.1109/ICORR.2011.5975340.

[11] M. Pan, C. Yuan, X. Liang, *et al.*, "Soft actuators and robotic devices for rehabilitation and assistance," *Advanced Intelligent Systems*, vol. 4, no. 4, p. 2 100 140, 2022. DOI: https://doi.org/10.1002/aisy.202100140. eprint: https://onlinelibrary.wiley.com/doi/pdf/10.1002/aisy.

202100140. [Online]. Available: https://onlinelibrary.wiley.com/doi/abs/10.1002/aisy.202100140.

[12] Flint Rehab, "Maximizing hand recovery after stroke: How to improve hand and finger mobility," Medicaly reviewd by Mariah Cairer PT, DPT, Dec. 2022.

[13] M. Yousufuddin and N. Young, "Aging and ischemic stroke," *Aging (Albany NY)*, vol. 11, no. 9, May 2019. DOI: 10.18632/aging.101931.

[14] T. Heart and E. Kalderon, "Older adults: Are they ready to adopt health-related ict?" *International journal of medical informatics*, vol. 82, no. 11, Nov. 2013. DOI: 10.1016/j.ijmedinf.2011.03.002.

[15] World Health Organization. "Social isolation and loneliness." (2023), [Online]. Available: https://www.who.int/teams/social-determinants-of-health/demographic-change-and-healthy-ageing/social-isolation-and-loneliness (visited on 02/01/2023).

[16] World Health Organization. "Determinants of health." (2017), [Online]. Available: https://www.who.int/news-room/questions-and-answers/item/determinants-of-health (visited on 02/01/2023).

[17] K. Dawson-Amoah and M. Varacallo, *Anatomy, Shoulder and Upper Limb, Hand Intrinsic Muscles*. StatPearls Publishing, 2022.

[18] M.-J. Liu, C.-H. Xiong, L. Xiong, and X.-L. Huang, "Biomechanical characteristics of hand coordination in grasping activities of daily living," *PLOS ONE*, vol. 11, no. 1, pp. 1–16, Jan. 2016. DOI: 10.1371/journal.pone.0146193. [Online]. Available: https://doi.org/10.1371/journal.pone.0146193.

[19] Y. Park, J. Lee, and J. Bae, "Development of a finger motion measurement system using linear potentiometers," in *2014 IEEE/ASME International Conference on Advanced Intelligent Mechatronics*, 2014, pp. 125–130. DOI: 10.1109/AIM.2014.6878066.

[20] P. Sherman, *German sign language letter sch*, [Online; accessed January 31, 2023], 2022. [Online]. Available: https://commons.wikimedia.org/wiki/File:German_Sign_Language_letter_SCH.svg.

[21] wpclipart.com, *Sign language a*, [Online; accessed January 31, 2023], 2016. [Online]. Available: https://www.wpclipart.com/sign_language/American_ABCs/a_labelled.png.html.

[22] Snailsmakemehappy, *Sign language 9*, [Online; accessed January 31, 2023], 2022. [Online]. Available: https://commons.wikimedia.org/wiki/File:Sign_language_9.jpg.

[23] Snailsmakemehappy, *Sign language 8*, [Online; accessed January 31, 2023], 2022. [Online]. Available: https://commons.wikimedia.org/wiki/File:Sign_language_8.jpg.

[24] Snailsmakemehappy, *Sign language 7*, [Online; accessed January 31, 2023], 2022. [Online]. Available: https://commons.wikimedia.org/wiki/File:Sign_language_7.jpg.

[25] Snailsmakemehappy, *Sign language 6*, [Online; accessed January 31, 2023], 2022. [Online]. Available: https://commons.wikimedia.org/wiki/File:Sign_language_6.jpg.

[26] G. Bain, N. Polites, B. Higgs, R. Heptinstall, and A. McGrath, "The functional range of motion of the finger joints," *Journal of Hand Surgery (European Volume)*, vol. 40, no. 4, pp. 406–411, 2015.

[27] M. C. Hume, H. Gellman, H. McKellop, and R. H. Brumfield Jr, "Functional range of motion of the joints of the hand," *The Journal of hand surgery*, vol. 15, no. 2, pp. 240–243, 1990.

[28] N. Smaby, M. E. Johanson, B. Baker, D. E. Kenney, W. M. Murray, and V. R. Hentz, "Identification of key pinch forces required to complete functional tasks.," *Journal of Rehabilitation Research & Development*, vol. 41, no. 2, 2004.

[29] B. Wang, A. McDaid, M. Biglari-Abhari, and K. C. Aw, "Design and development of a glove for post-stroke hand rehabilitation," in *2017 IEEE international conference on advanced intelligent mechatronics (AIM)*, IEEE, 2017, pp. 1047–1051.

[30] M. Li, A. Pal, A. Aghakhani, A. Pena-Francesch, and M. Sitti, "Soft actuators for real-world applications," *Nature Reviews Materials*, vol. 7, no. 1, pp. 17–44, Jan. 2022, Review Article, ISSN: 2058-8437. DOI: 10.1038/s41578-021-00389-7.

[31] M. Li, A. Pal, A. Aghakhani, and et al., "Soft actuators for real-world applications," *Nat Rev Mater*, vol. 7, pp. 235–249, Mar. 2022, Accepted: 21 September 2021, Published: 10 November 2021. DOI: 10.1038/s41578-021-00389-7. [Online]. Available: https://doi.org/10.1038/s41578-021-00389-7.

[32] P. Polygerinos, S. Lyne, Z. Wang, *et al.*, "Towards a soft pneumatic glove for hand rehabilitation," in *2013 IEEE/RSJ International Conference on Intelligent Robots and Systems (IROS)*, IEEE, Nov. 2013. [Online]. Available: https://ieeexplore.ieee.org/stamp/stamp.jsp?tp=&arnumber=6696549.

[33] G. Klute, J. Czerniecki, and B. Hannaford, "Mckibben artificial muscles: Pneumatic actuators with biomechanical intelligence," in *1999 IEEE/ASME International Conference on Advanced Intelligent Mechatronics (Cat. No.99TH8399)*, 1999, pp. 221–226. DOI: 10.1109/AIM.1999.803170.

[34] W. Zhao, H. Xu, Y. Ma, and Y. Xu, "Design and experimental test of the contractive and elongate water hydraulic flexible manipulators," in *2017 IEEE International Conference on Robotics and Biomimetics (ROBIO)*, 2017, pp. 1503–1508. DOI: 10.1109/ROBIO.2017.8324630.

[35] R. Hashem, M. Stommel, L. K. Cheng, and W. Xu, "Design and characterization of a bellows-driven soft pneumatic actuator," *IEEE/ASME Transactions on Mechatronics*, vol. 26, no. 5, pp. 2327–2338, Oct. 2021. DOI: 10.1109/TMECH.2020.3037643.

[36] G. Decroly, B. Mertens, P. Lambert, *et al.*, "Design, characterization and optimization of a soft fluidic actuator for minimally invasive surgery," *Int J CARS*, vol. 15, pp. 333–340, 2020. DOI: https://doi.org/10.1007/s11548-019-02081-2.

[37] K. Sun and Y. Tian, "Numerical investigation of a bioinspired multi-segment soft pneumatic actuator for grasping applications," *Materials Today Com-*

munications, vol. 31, p. 103 449, 2022, ISSN: 2352-4928. DOI: https://doi.org/10.1016/j.mtcomm.2022.103449.

[38] G. Chen, X. Yang, X. Zhang, and H. Hu, "Water hydraulic soft actuators for underwater autonomous robotic systems," *Applied Ocean Research*, vol. 109, p. 102 551, 2021, ISSN: 0141-1187. DOI: https://doi.org/10.1016/j.apor.2021.102551.

[39] T. Wang, L. Ge, and G. Gu, "Programmable design of soft pneu-net actuators with oblique chambers can generate coupled bending and twisting motions," *Sensors and Actuators A: Physical*, vol. 271, pp. 131–138, 2018, ISSN: 0924-4247. DOI: https://doi.org/10.1016/j.sna.2018.01.018.

[40] S. Coyle, C. Majidi, P. LeDuc, and K. J. Hsia, "Bio-inspired soft robotics: Material selection, actuation, and design," *Scientific Reports*, 2017. DOI: https://doi.org/10.1016/j.eml.2018.05.003.

[41] M. Ariyanto, J. D. Setiawan, R. Ismail, I. Haryanto, T. Febrina, and D. R. Saksono, "Design and characterization of low-cost soft pneumatic bending actuator for hand rehabilitation," in *2018 5th International Conference on Information Technology, Computer, and Electrical Engineering (ICITACEE)*, 2018, pp. 45–50. DOI: 10.1109/ICITACEE.2018.8576909.

[42] Y. Sun, Y. S. Song, and J. Paik, "Characterization of silicone rubber based soft pneumatic actuators," *Scientific Reports*, 2013. DOI: 10.1109/IROS.2013.6696995.

[43] N. Gariya, P. Kumar, and B. Prasad, "Stress and bending analysis of a soft pneumatic actuator considering different hyperelastic materials," *Materials Today: Proceedings*, vol. 65, pp. 3126–3131, 2022, 2022 International Conference on Materials and Sustainable Manufacturing Technology, ISSN: 2214-7853. DOI: https://doi.org/10.1016/j.matpr.2022.05.352. [Online]. Available: https://www.sciencedirect.com/science/article/pii/S2214785322036434.

[44] E. Acome, S. K. Mitchell, T. G. Morrissey, *et al.*, "Hydraulically amplified self-healing electrostatic actuators with muscle-like performance," *Science*, vol. 359, no. 6371, pp. 61–65, 2018. DOI: 10.1126/science.aao6139.

[45] E. Hajiesmailia and D. R. Clarke, "Dielectric elastomer actuators featured," *Journal of Applied Physics*, vol. 129, no. 151102, pp. 1–6, 2021. DOI: 10.1063/5.0043959.

[46] N. Kellaris, V. G. Venkata, P. Rothemund, and C. Keplinger, "An analytical model for the design of peano-hasel actuators with drastically improved performance," *Extreme Mechanics Letters*, vol. 30, p. 100 449, 2019, Available online 29 March 2019, ISSN: 2352-4316. DOI: 10.1016/j.eml.2019.100449.

[47] K. Mizushima, T. Oku, Y. Suzuki, T. Tsuji, and T. Watanabe, "Multi-fingered robotic hand based on hybrid mechanism of tendon-driven and jamming transition," in *2018 IEEE International Conference on Soft Robotics (RoboSoft)*, Apr. 2018, pp. 376–381. DOI: 10.1109/ROBOSOFT.2018.8404948.

[48] U. Jeong, H. In, H. Lee, B. B. Kang, and K.-J. Cho, "Investigation on the control strategy of soft wearable robotic hand with slack enabling tendon actuator," in *2015 IEEE International Conference on Robotics and Automation (ICRA)*, 2015, pp. 5004–5009. DOI: 10.1109/ICRA.2015.7139895.

[49] H.-I. Kim, M.-W. Han, S.-H. Song, and S.-H. Ahn, "Soft morphing hand driven by sma tendon wire," *Composites Part B: Engineering*, vol. 105, pp. 138–148, 2016, ISSN: 1359-8368. DOI: https://doi.org/10.1016/j.compositesb.2016.09.004. [Online]. Available: https://www.sciencedirect.com/science/article/pii/S1359836816318510.

[50] Y. Haibin, K. Cheng, L. Junfeng, and Y. Guilin, "Modeling of grasping force for a soft robotic gripper with variable stiffness," *Mechanism and Machine Theory*, vol. 128, pp. 254–274, 2018, ISSN: 0094-114X. DOI: https://doi.org/10.1016/j.mechmachtheory.2018.05.005. [Online]. Available: https://www.sciencedirect.com/science/article/pii/S0094114X17314957.

[51] J. Lee, Y. Chung, and H. Rodrigue, "Long shape memory alloy tendon-based soft robotic actuators and implementation as a soft gripper," *Scientific Reports*, vol. 9, no. 11251, 2019. DOI: 10.1038/s41598-019-47794-1.

[52] V. jagota, A. Sethi, and D.-K. Kumar, "Finite element method: An overview," *Walailak Journal of Science Technology*, vol. 10, pp. 1–8, Jan. 2013. DOI: 10.2004/wjst.v10i1.499.

[53] Ansys, *Ansys mechanical finite element analysis (fea) software for structural engineering*, Jan. 2023. [Online]. Available: https://www.ansys.com/products/structures/ansys-mechanical.

[54] Z. Sun, Z.-h. Guo, and W. Tang, "Design of wearable hand rehabilitation glove with soft hoop-reinforced pneumatic actuator," *Journal of Central South University*, vol. 26, pp. 106–119, Jan. 2019. DOI: 10.1007/s11771-019-3986-x.

[55] H. K. Yap, J. H. Lim, F. Nasrallah, J. C. H. Goh, and R. C. H. Yeow, "A soft exoskeleton for hand assistive and rehabilitation application using pneumatic actuators with variable stiffness," in *2015 IEEE International Conference on Robotics and Automation (ICRA)*, 2015, pp. 4967–4972. DOI: 10.1109/ICRA.2015.7139889.

[56] P. Polygerinos, K. C. Galloway, E. Savage, M. Herman, K. O. Donnell, and C. J. Walsh, "Soft robotic glove for hand rehabilitation and task specific training," in *2015 IEEE International Conference on Robotics and Automation (ICRA)*, 2015, pp. 2913–2919. DOI: 10.1109/ICRA.2015.7139597.

[57] H. K. Yap, J. Cho, and R. C.-H. Yeow, "Design and characterization of soft actuator for hand rehabilitation application," vol. 45, Sep. 2014, ISBN: 978-3-319-11127-8. DOI: 10.1007/978-3-319-11128-5_92.

[58] Z. Q. Tang, H. L. Heung, K. Y. Tong, and Z. Li, "Model-based online learning and adaptive control for a "human-wearable soft robot" integrated system," *The International Journal of Robotics Research*, vol. 40, no. 1, pp. 256–276, 2021. DOI: 10.1177/0278364919873379. eprint: https://doi.org/10.1177/0278364919873379. [Online]. Available: https://doi.org/10.1177/0278364919873379.

[59] K. Elgeneidy, N. Lohse, and M. Jackson, "Bending angle prediction and control of soft pneumatic actuators with embedded flex sensors – a data-driven approach," *Mechatronics*, vol. 50, pp. 234–247, 2018, ISSN: 0957-4158. DOI: https://doi.org/10.1016/j.mechatronics.2017.10.005. [Online].

Available: https://www.sciencedirect.com/science/article/pii/S0957415817301496.

[60] J. Walker, T. Zidek, C. Harbel, *et al.*, "Soft robotics: A review of recent developments of pneumatic soft actuators," *Actuators*, vol. 9, no. 1, 2020, ISSN: 2076-0825. DOI: 10.3390/act9010003. [Online]. Available: https://www.mdpi.com/2076-0825/9/1/3.

[61] T. Sugiyama, K. Kutsuzawa, D. Owaki, and M. Hayashibe, "Individual deformability compensation of soft hydraulic actuators through iterative learning-based neural network," *Bioinspiration / Biomimetics*, vol. 16, p. 056 016, Aug. 2021. DOI: 10.1088/1748-3190/ac1b6f.

[62] S. Gunnarsson and M. Norrlöf, "A short introduction to iterative learning control," Linköping University, The Institute of Technology, Tech. Rep. 1926, 1997, p. 16.

[63] S. Balasubramanian, R. Wei, M. Perez, *et al.*, "Rupert: An exoskeleton robot for assisting rehabilitation of arm functions," *2008 Virtual Rehabilitation*, pp. 163–167, 2008.

[64] G. Ellis, "Chapter 6 - four types of controllers," in *Control System Design Guide (Fourth Edition)*, G. Ellis, Ed., Fourth Edition, Boston: Butterworth-Heinemann, 2012, pp. 97–119, ISBN: 978-0-12-385920-4. DOI: https://doi.org/10.1016/B978-0-12-385920-4.00006-0. [Online]. Available: https://www.sciencedirect.com/science/article/pii/B9780123859204000060.

[65] N. Nasri, S. Orts-Escolano, and M. Cazorla, "An sEMG-Controlled 3D Game for Rehabilitation Therapies: Real-Time Time Hand Gesture Recognition Using Deep Learning Techniques," *Sensors*, vol. 20, no. 22, p. 6451, Nov. 2020. DOI: 10.3390/s20226451. [Online]. Available: https://doi.org/10.3390/s20226451.

[66] J. J. A. Mendes Junior, C. E. Pontim, T. S. Dias, and D. P. Campos, "How do semg segmentation parameters influence pattern recognition process? an approach based on wearable semg sensor," *Biomedical Signal Processing and Control*, vol. 81, p. 104 546, 2023, ISSN: 1746-8094. DOI: https://doi.org/10.1016/j.bspc.2022.104546. [Online]. Available: https://www.sciencedirect.com/science/article/pii/S174680942201000X.

[67] S. Rawat, S. Vats, and P. Kumar, "Evaluating and exploring the myo armband," in *2016 International Conference System Modeling / Advancement in Research Trends (SMART)*, 2016, pp. 115–120. DOI: 10.1109/SYSMART.2016.7894501.

[68] G. D. Morais, L. C. Neves, A. A. Masiero, and M. C. F. de Castro, "Application of myo armband system to control a robot interface.," *BIOSIGNALS*, vol. 4, pp. 227–231, 2016.

[69] P. Walkington, *PyoMyo*, version 0.0.5, Nov. 2021. [Online]. Available: https://github.com/PerlinWarp/pyomyo.

[70] J. Zea, M. E. Benalcázar, L. I. Barona Lôpez, and Á. L. Valdivieso Caraguay, "An open-source data acquisition and manual segmentation system for hand gesture recognition based on emg," in *2021 IEEE Fifth Ecuador Technical Chapters Meeting (ETCM)*, 2021, pp. 1–6. DOI: 10.1109/ETCM53643.2021.9590811.

[71] Y. Liu, C. Lin, and Z. Li, "Wr-hand: Wearable armband can track user's hand," *Proc. ACM Interact. Mob. Wearable Ubiquitous Technol.*, vol. 5, no. 3, Sep. 2021. DOI: 10.1145/3478112. [Online]. Available: https://doi.org/10.1145/3478112.

[72] M. Fiala, "Artag, a fiducial marker system using digital techniques," in *2005 IEEE Computer Society Conference on Computer Vision and Pattern Recognition (CVPR'05)*, vol. 2, 2005, 590–596 vol. 2. DOI: 10.1109/CVPR.2005.74.

[73] L. Calvet, P. Gurdjos, C. Griwodz, and S. Gasparini, "Detection and accurate localization of circular fiducials under highly challenging conditions," in *Proceedings of the IEEE Conference on Computer Vision and Pattern Recognition*, 2016, pp. 562–570.

[74] G. Bradski, "The OpenCV Library," *Dr. Dobb's Journal of Software Tools*, 2000.

[75] Trafikverket, *Mätning av ljudnivå*, Senast uppdaterad/granskad: 2020-11-10, 2020. [Online]. Available: https://bransch.trafikverket.se/for-dig-i-branschen/miljo---for-dig-i-branschen/buller-och-vibrationer---for-dig-i-branschen/Fakta-om-buller-och-vibrationer/matt-for-ljudnivaer/.

[76] D. Wang, Z.-y. Li, and Y.-q. Zhu, "Lubrication and tribology in seawater hydraulic piston pump," *Journal of Marine Science and Application*, vol. 2, no. 1, pp. 35–40, 2003, ISSN: 1993-5048. DOI: 10.1007/BF02935573. [Online]. Available: https://doi.org/10.1007/BF02935573.

[77] M. Focchi, E. Guglielmino, C. Semini, *et al.*, "Water/air performance analysis of a fluidic muscle," *Scientific Reports*, vol. 9, no. 11251, 2019. DOI: 10.1109/IROS.2010.5650432.

[78] D. Caldwell, G. Medrano-Cerda, and M. Goodwin, "Control of pneumatic muscle actuators," *IEEE Control Systems Magazine*, vol. 15, no. 1, pp. 40–48, 1995. DOI: 10.1109/37.341863.

[79] M. Gannon, *Aeration vs. cavitation in hydraulic system design*. [Online]. Available: https://www.fluidpowerworld.com/aeration-versus-cavitation/ (visited on 02/02/2023).

[80] F. Daerden and D. Lefeber, "Water/air performance analysis of a fluidic muscle," *Scientific Reports*, vol. 47, no. 1, 2002. DOI: 10.1038/s41598-019-47794-1.

[81] M. Zinn, O. Khatib, B. Roth, and J. Salisbury, "Actuation methods for human-centered robotics and associated control challenges," *Scientific Reports*, vol. 9, no. 11251, 2019. DOI: 10.1038/s41598-019-47794-1.

[82] A. A. M. Faudzi, M. R. M. Razif, I. N. A. M. Nordin, K. Suzumori, S. Wakimoto, and D. Hirooka, "Development of bending soft actuator with different braided angles," in *2012 IEEE/ASME International Conference on Advanced Intelligent Mechatronics (AIM)*, 2012, pp. 1093–1098. DOI: 10.1109/AIM.2012.6266037.

[83] M. S. Xavier, A. J. Fleming, and Y. K. Yong, "Modelling and simulation of pneumatic sources for soft robotic applications," in *2020 IEEE/ASME International Conference on Advanced Intelligent Mechatronics (AIM)*, 2020, pp. 916–921. DOI: 10.1109/AIM43001.2020.9158802.

[84] J. Jørgensen Soft robotics toolkit. "Syringe actuation and arduino control." (2023), [Online]. Available: https://softroboticstoolkit.com/laser-cut-molds/controls-actuation/actuation-controls (visited on 03/29/2023).

[85] A. Shrivastava. "Programmable-air." (), [Online]. Available: https://www.programmableair.com/ (visited on 04/03/2023).

[86] E. Y. Wu, *Syringecontrolsystem*, 2020. [Online]. Available: https://github.com/EricYufengWu/SyringeControlSystem (visited on 04/17/2023).

[87] M. Li, T. Wang, Y. Zhuo, *et al.*, "A soft robotic glove for hand rehabilitation training controlled by movements of the healthy hand," in *2020 17th International Conference on Ubiquitous Robots (UR)*, 2020, pp. 62–67. DOI: 10.1109/UR49135.2020.9144753.

[88] X. Cao, K. Ma, Z. Jiang, and F. Xu, "A soft robotic glove for hand rehabilitation using pneumatic actuators with jamming structure," in *2021 40th Chinese Control Conference (CCC)*, 2021, pp. 4120–4125. DOI: 10.23919/CCC52363.2021.9550076.

[89] J. Wang, Y. Fei, and W. Pang, "Design, modeling, and testing of a soft pneumatic glove with segmented pneunets bending actuators," *IEEE/ASME Transactions on Mechatronics*, vol. 24, no. 1, pp. 121–131, Feb. 2019, Design, Modeling, and Testing of a Soft Pneumatic Glove With Segmented PneuNets Bending Actuators, ISSN: 1083-4435. DOI: 10.1109/TMECH.2018.2885263. [Online]. Available: https://ieeexplore.ieee.org/document/8693775.

[90] Occupational Safety and Health Standards, *Hand and portable powered tools and equipment, general*, 29 C.F.R. § 1910 Subpart P, GPO Source:e-CFR, 2021.

[91] S. Dilibal, H. Sahin, and Y. Celik, "Experimental and numerical analysis on the bending response of the geometrically gradient soft robotics actuator," *Archives of Mechanics*, vol. 70, no. 5, pp. 391–404, 2018. DOI: 10.24423/aom.2903.

[92] SAM Outillage, *SYRINGE FOR BRAKE FLUID FILLING*, https://www.sam-outillage.com/outil-syringe-for-brake-fluid-filling-73125.htm, Accessed May 4, 2023.

[93] Actuonix Motion Devices, *Actuonix l16-140-35-12-p*, https://www.actuonix.com/l16-140-35-12-p, Accessed: May 4, 2023, n.d.

[94] Weihong Guan and Bogdan Necula, *HX711*, https://github.com/bogde/HX711, 2022.

[95] E. Werner, *Honeywell TruStability SPI*, https://github.com/huilab/HoneywellTruStabilitySPI, Hui Lab, 2019.

[96] Z. Liu, F. Wang, S. Liu, Y. Tian, and D. Zhang, "Modeling and analysis of soft pneumatic network bending actuators," *IEEE/ASME Transactions on Mechatronics*, vol. 26, no. 4, pp. 2195–2203, 2021. DOI: 10.1109/TMECH.2020.3034640.

[97] Y. Sun, Q. Zhang, X. Chen, and H. Chen, "An optimum design method of pneu-net actuators for trajectory matching utilizing a bending model and ga," *Mathematical Problems in Engineering*, vol. 2019, p. 6 721 897, 2019, ISSN: 1024-123X. DOI: 10.1155/2019/6721897. [Online]. Available: https://doi.org/10.1155/2019/6721897.

[98] P. Polygerinos, Z. Wang, J. T. Overvelde, *et al.*, "Modeling of soft fiber-reinforced bending actuators," *IEEE Transactions on Robotics*, vol. 31, no. 3, pp. 778–789, 2015. DOI: 10.1109/TRO.2015.2428504.

[99] R. Chen, Y. Jia, Y. Li, and J. Pan, "Modeling and analysis of fiber-reinforced soft bending actuators," *IEEE Access*, vol. 9, pp. 56 568–56 577, 2021. DOI: 10.1109/PESA50370.2020.9343954.

[100] *Ease release™ 200 product information*, accessed May 4, 2023. [Online]. Available: https://www.smooth-on.com/products/ease-release-200/.

[101] *Silicone thinner™ product information*, Website, Smooth-On. [Online]. Available: https://www.smooth-on.com/products/silicone-thinner/ (visited on 05/04/2023).

[102] *Ecoflex™ gel 2 product information*, May n.d. [Online]. Available: https://www.smooth-on.com/products/ecoflex-gel-2/.

[103] *Dragon skin™ fx-pro™ product information*, accessed May 4, 2023. [Online]. Available: https://www.smooth-on.com/products/dragon-skin-fx-pro/.

[104] "Dragon skin™ 20 product information." Accessed May 4, 2023. (), [Online]. Available: https://www.smooth-on.com/products/dragon-skin-20/.

[105] *Dragon skin™ 30 product information*, Accessed May 4, 2023, May n.d. [Online]. Available: https://www.smooth-on.com/products/dragon-skin-30/.

[106] I. Smooth-On, *Smooth-sil™ 945 product information | smooth-on, inc.* https://www.smooth-on.com/products/smooth-sil-945/, Accessed: May 4, 2023, May 2023. [Online]. Available: https://www.smooth-on.com/products/smooth-sil-945/.

[107] Arbetsmiljöverket, *Buller*, Version 2.4.0, 2022. [Online]. Available: https://www.av.se/halsa-och-sakerhet/buller/mata-ljud-och-buller/mat-buller-med-din-mobiltelefon/.

[108] W. Park, S. Seo, and J. Bae, "A hybrid gripper with soft material and rigid structures," *IEEE Robotics and Automation Letters*, vol. 4, no. 1, p. 65, Jan. 2019. DOI: 10.1109/LRA.2018.2878972.

[109] *Sil-poxy™ product information*, Website, Smooth-On. [Online]. Available: https://www.smooth-on.com/products/sil-poxy/ (visited on 05/12/2023).

A

Appendix 1

A.1 Motion traces and Angles from all measurements

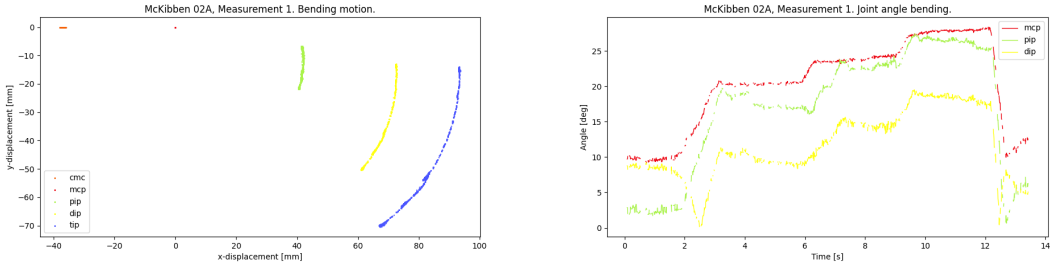

(a) Motion **(b)** Angles

Figure A.1: McKibben 02A, measurement 1.

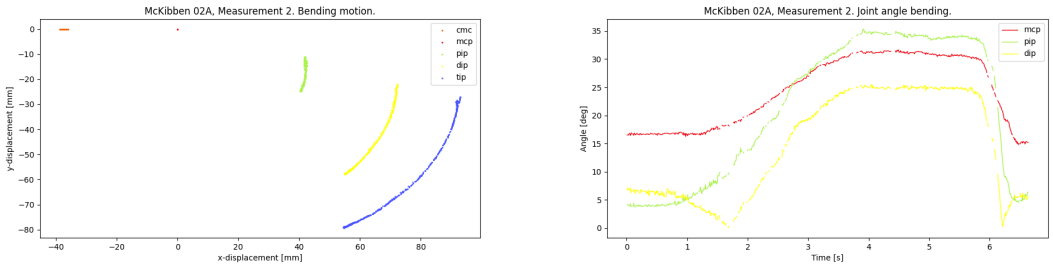

(a) Motion **(b)** Angles

Figure A.2: McKibben 02A, measurement 2.

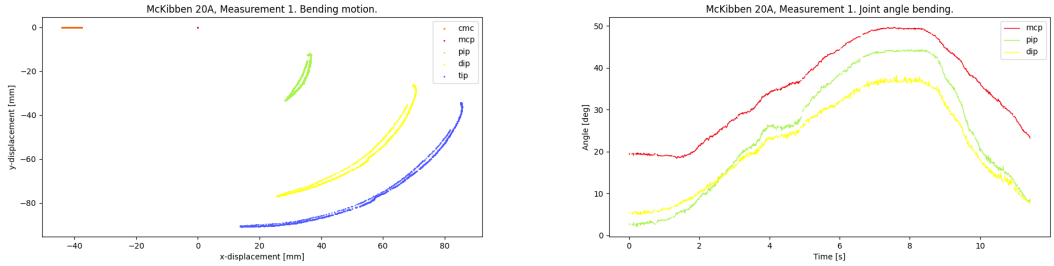

(a) Motion **(b)** Angles

Figure A.3: McKibben 20A, measurement 1.

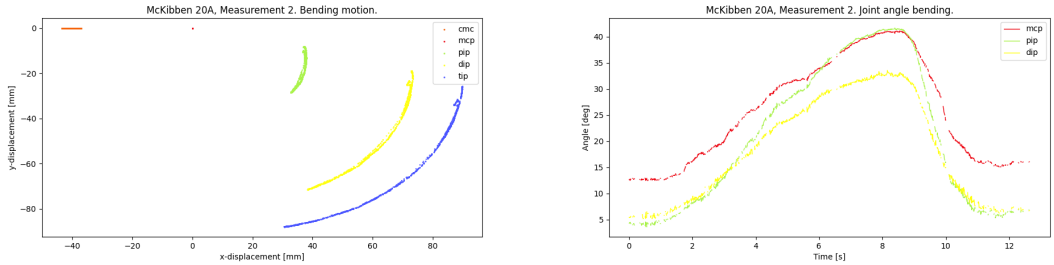

(a) Motion **(b)** Angles

Figure A.4: McKibben 20A, measurement 2.

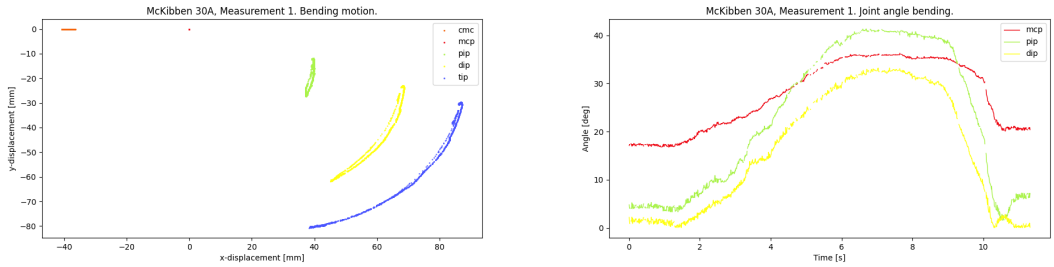

(a) Motion **(b)** Angles

Figure A.5: McKibben 30A, measurement 1.

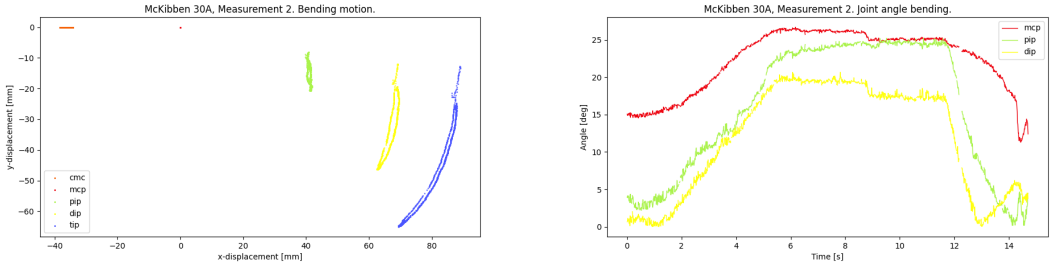

(a) Motion **(b)** Angles

Figure A.6: McKibben 30A, measurement 2.

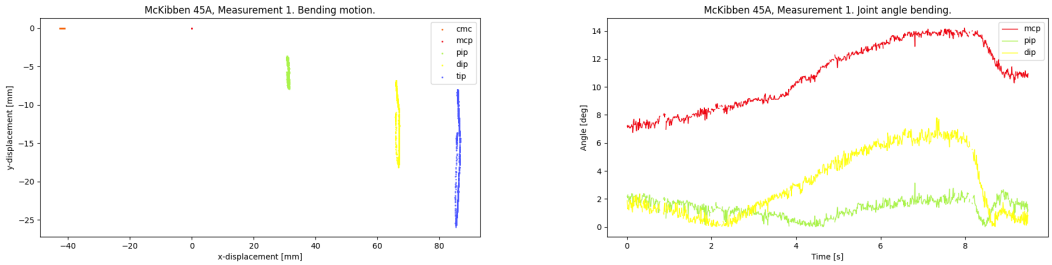

(a) Motion **(b)** Angles

Figure A.7: McKibben 45A, measurement 1.

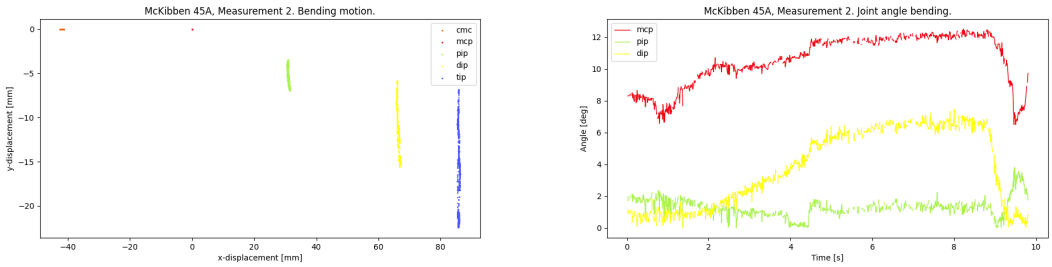

(a) Motion **(b)** Angles

Figure A.8: McKibben 45A, measurement 2.

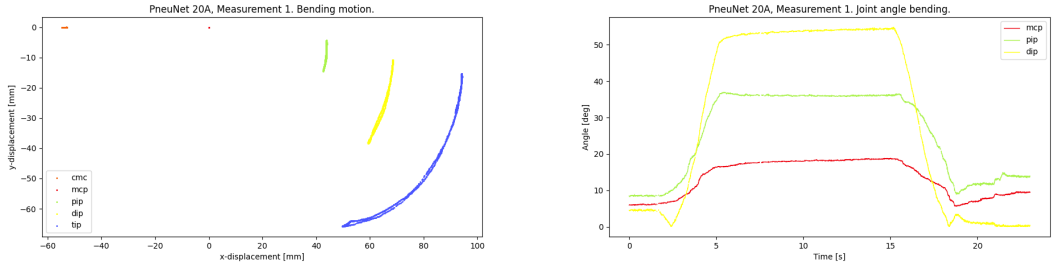

(a) Motion **(b)** Angles

Figure A.9: PneuNet 20A, measurement 1.

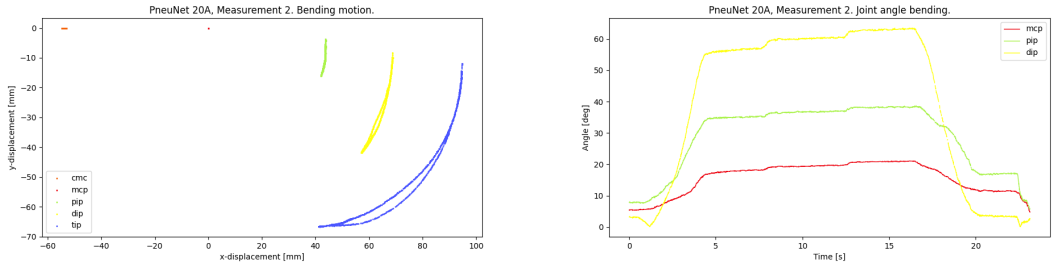

(a) Motion **(b)** Angles

Figure A.10: PneuNet 20A, measurement 2.

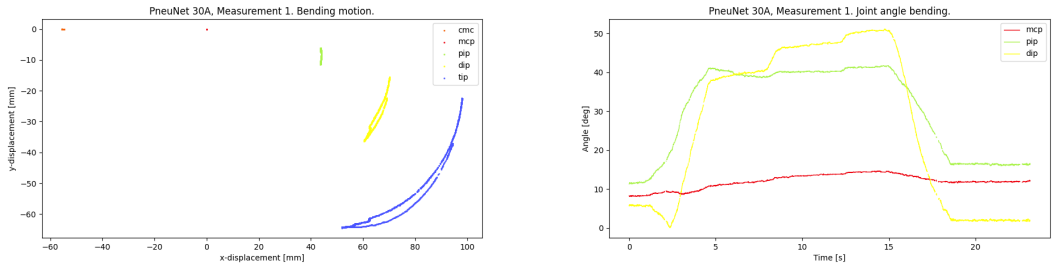

(a) Motion **(b)** Angles

Figure A.11: PneuNet 30A, measurement 1.

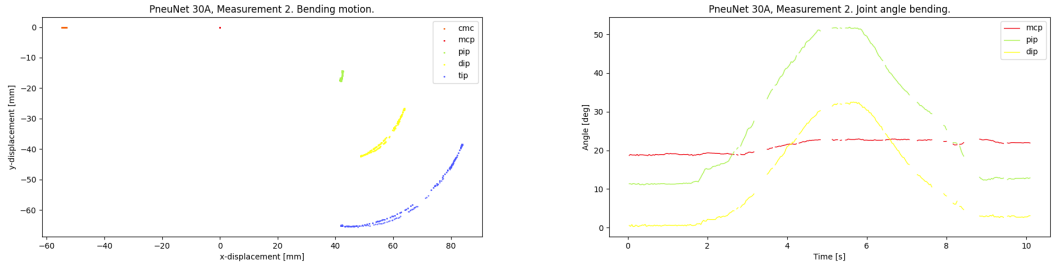

(a) Motion **(b)** Angles

Figure A.12: PneuNet 30A, measurement 2.

DEPARTMENT OF ELECTRICAL ENGINEERING
CHALMERS UNIVERSITY OF TECHNOLOGY
Gothenburg, Sweden
www.chalmers.se

CHALMERS
UNIVERSITY OF TECHNOLOGY